Self-Assembly

*The **spontaneous and reversible** association of molecular species to form larger, more complex supramolecular entities according to the **intrinsic information** contained in the components.*

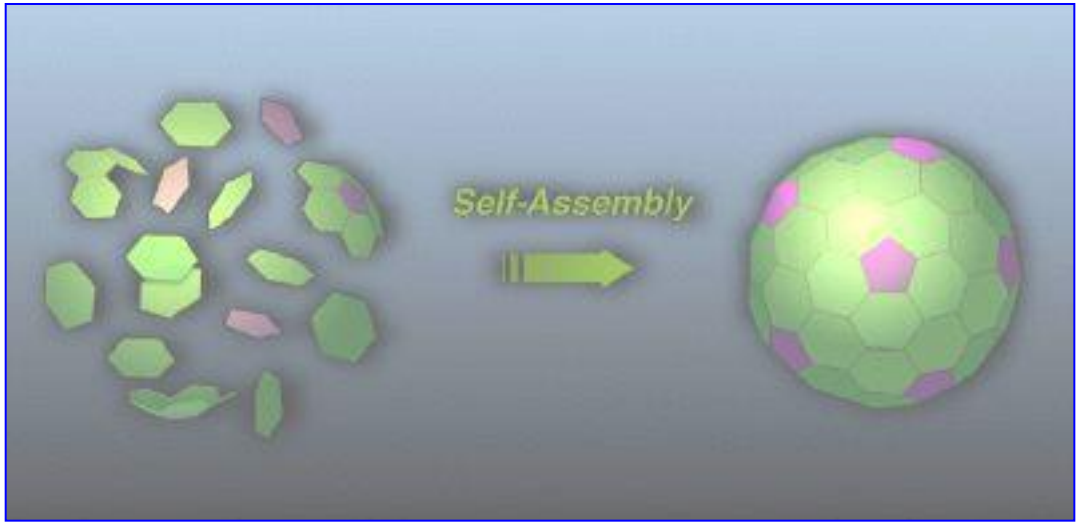

Supramolecular Coordination Chemistry

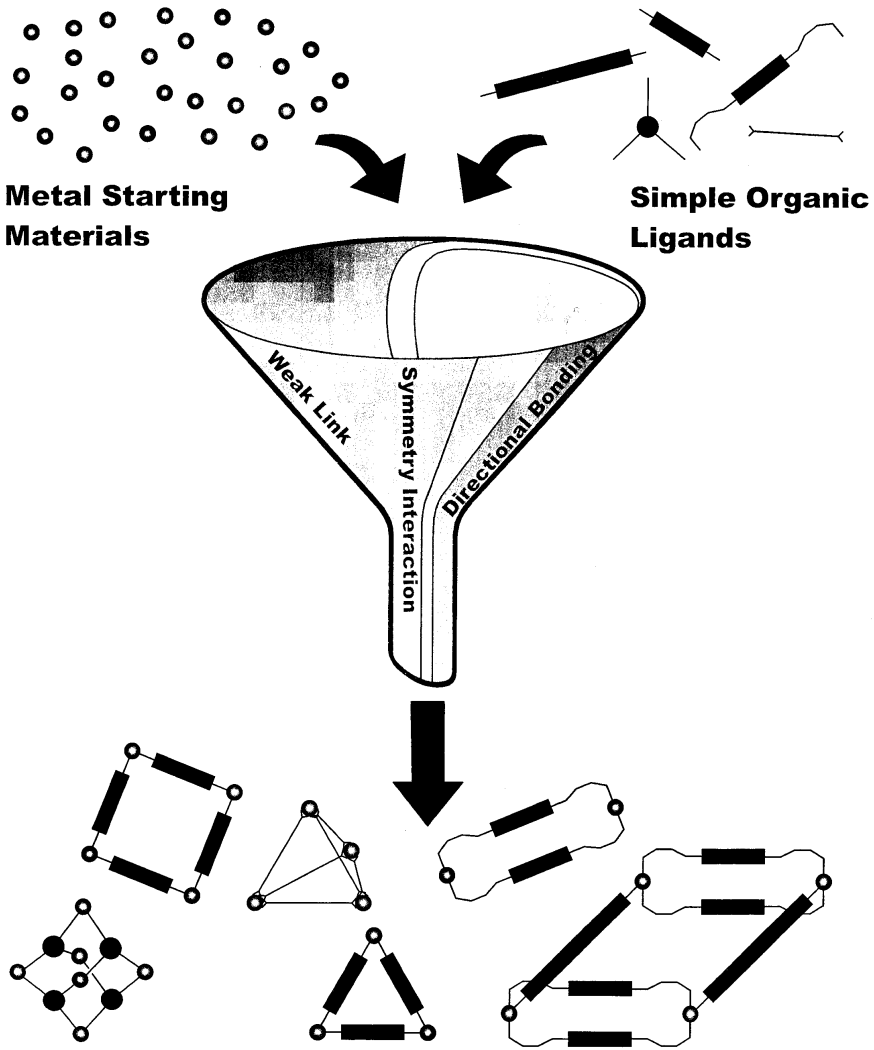

Metal as **connector** :

- labile M-L interaction (kinetic)
- stable compound (thermodynamic)
- highly directional with many geometries available

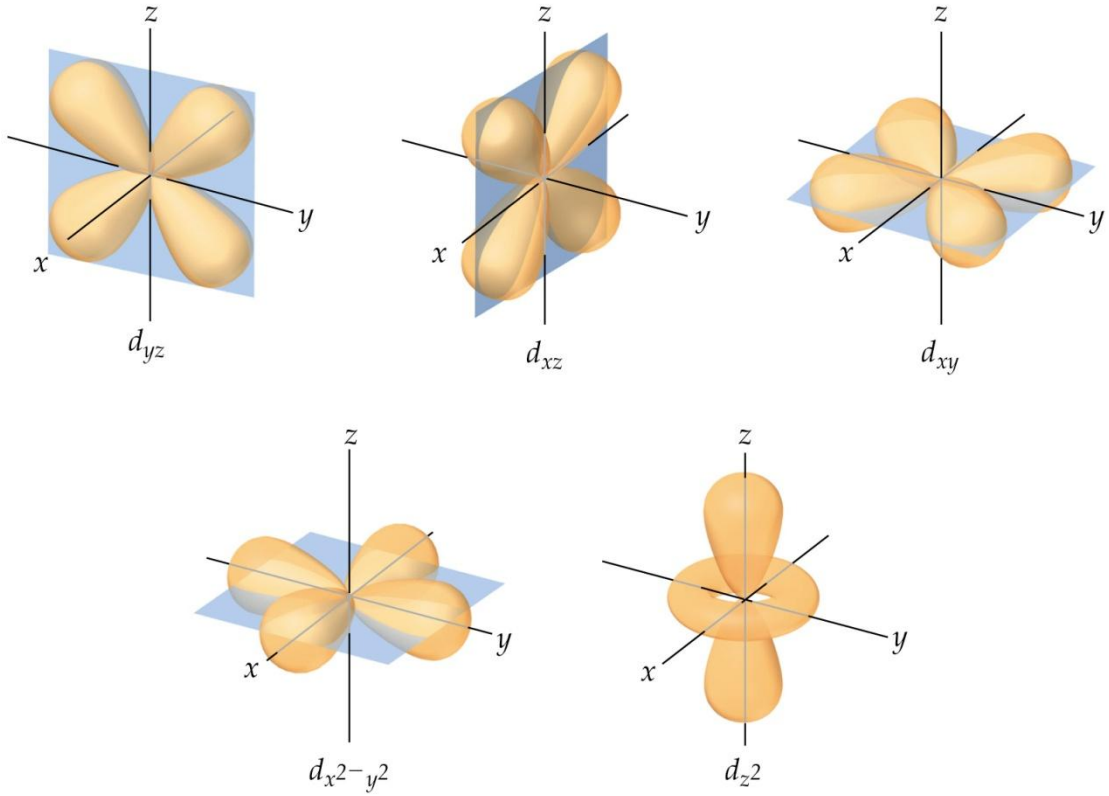

Metal as **functional group** :

- redox active (electron transfer)
- UV-vis active (color)
- photo active (phosphorescence)
- magnetic properties

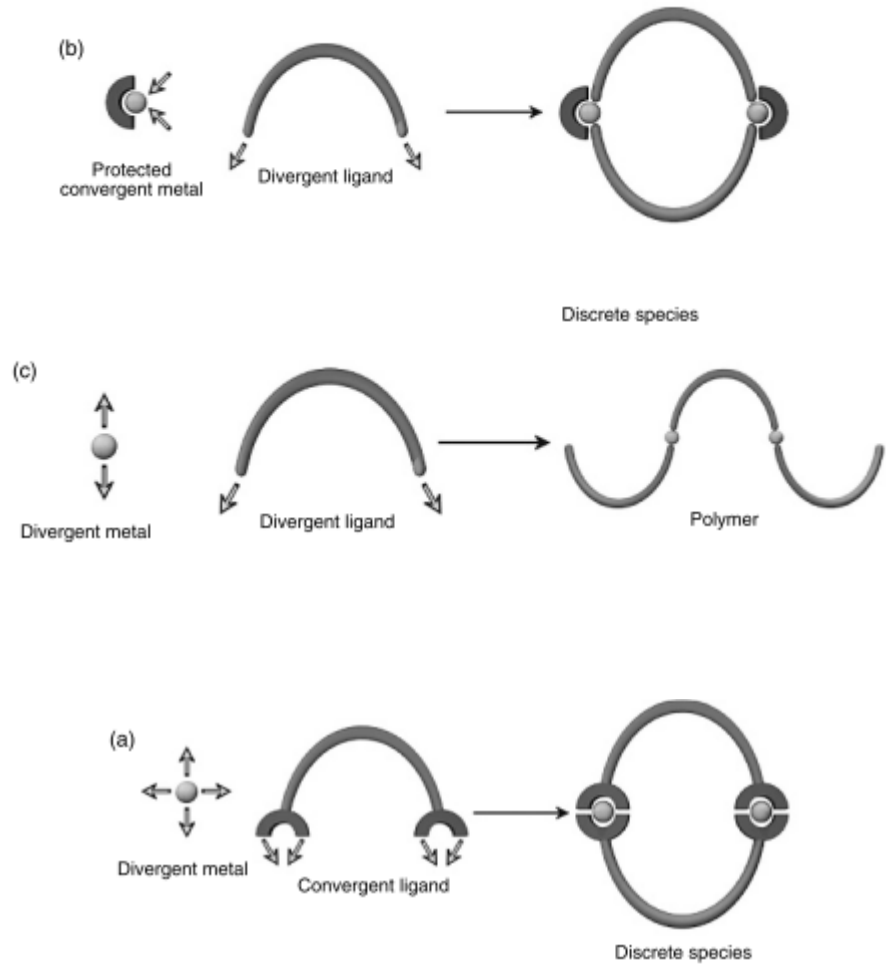
(b)
Protected convergent metal
Divergent ligand
Discrete species
(c)
Divergent metal
Divergent ligand
Polymer
(a)
Divergent metal
Convergent ligand
Discrete species

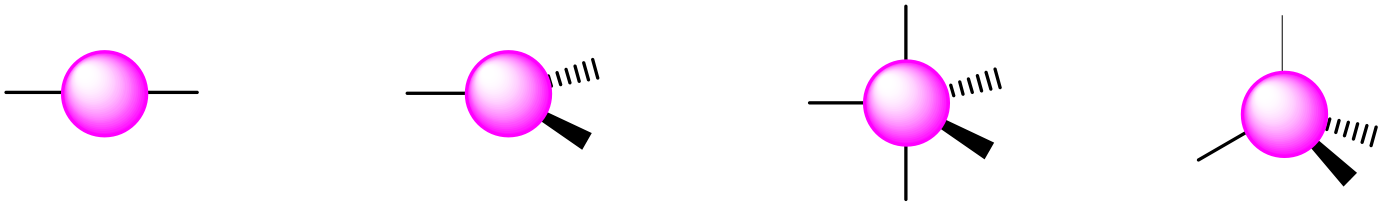

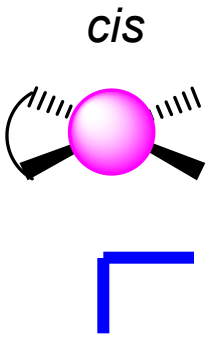

Classical metals used:

Pd(II), Pt(II), Cu(I), Cu(II), Re(I), Co(II), Fe(II), Ag(I), Zn(II), Ru(II)…

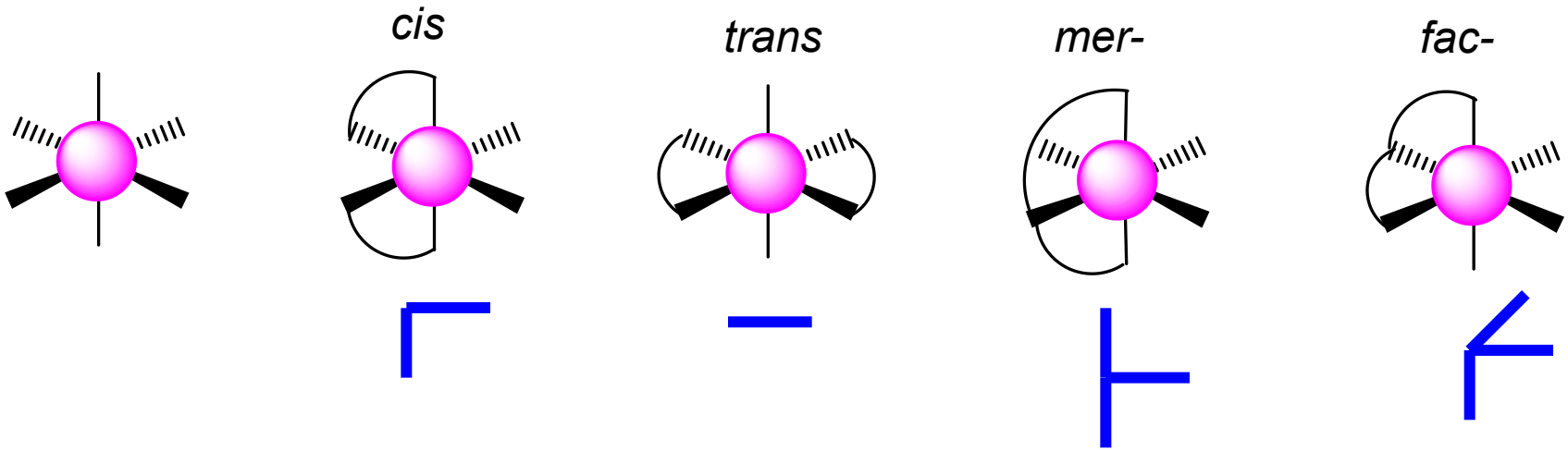

Directonal Bonding Approach

M = bb acido, **L** = bb basico, definiti secondo il numero e geometria relativa dei siti acidi e basici

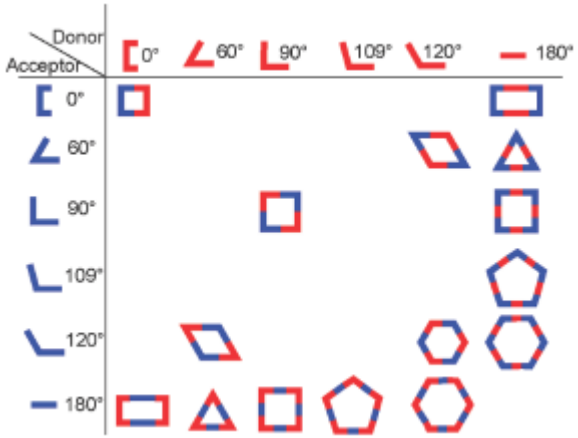

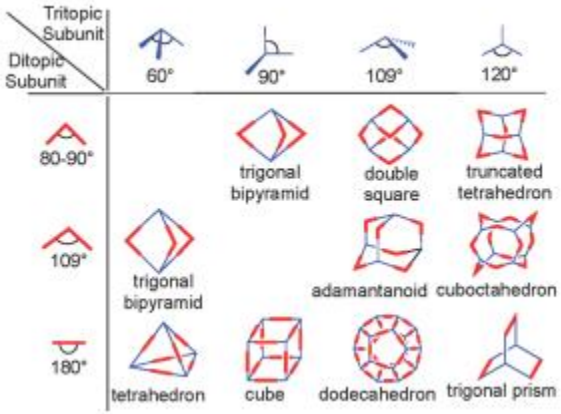

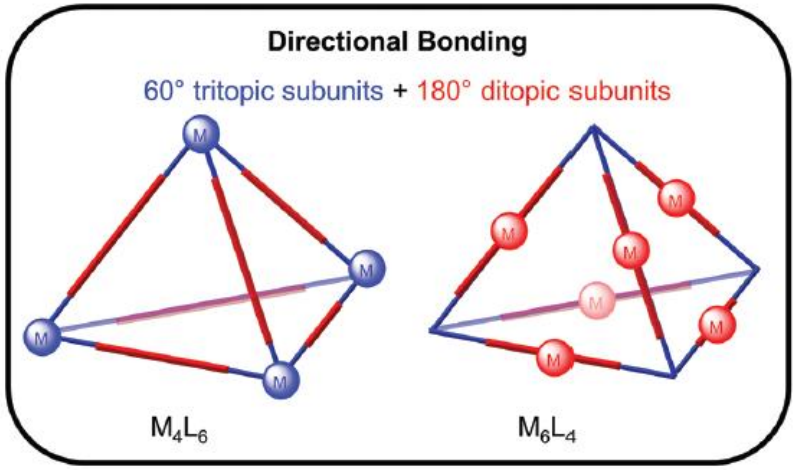
Directional Bonding
60° tritopic subunits + 180° ditopic subunits
M
M_4L_6
M_6L_4

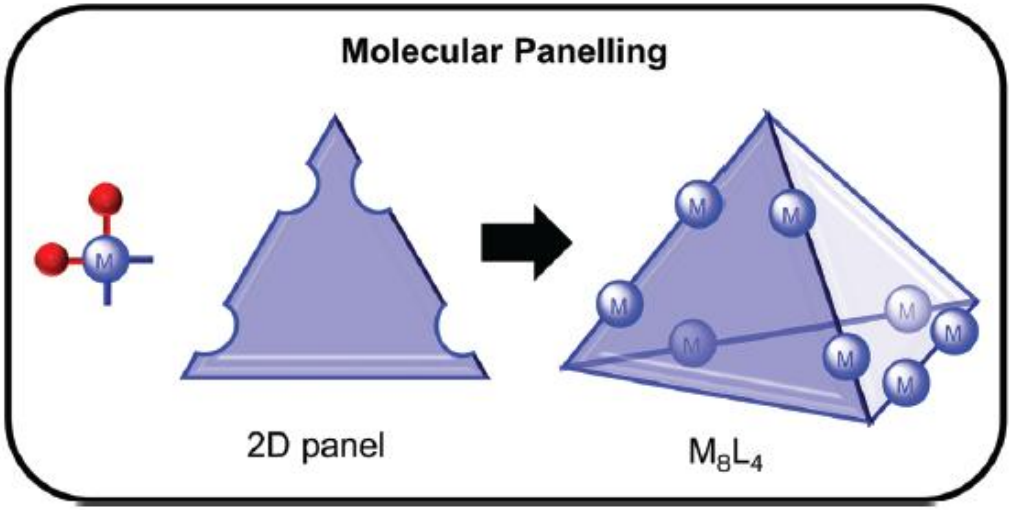
Molecular Panelling
M
2D panel
M_8L_4

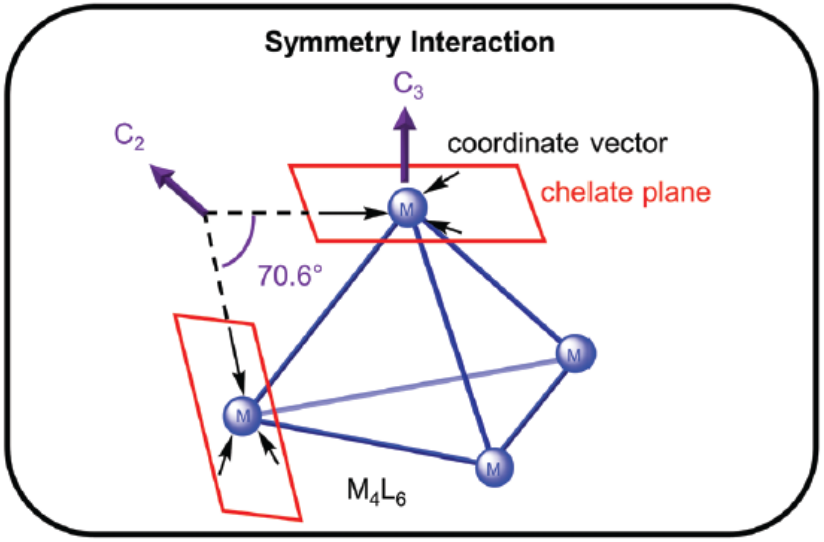

Banana-shaped ligands

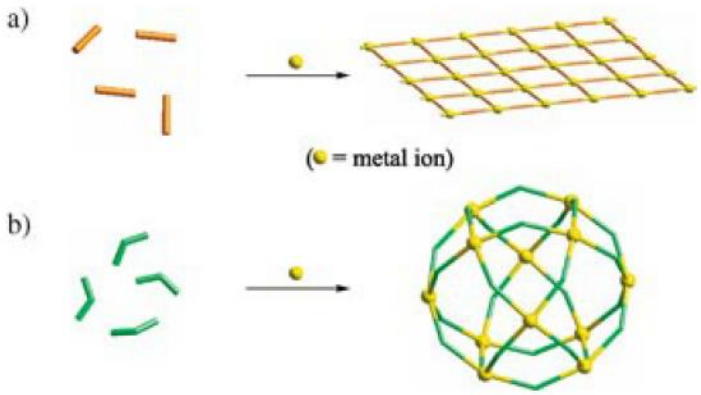

2D discrete species

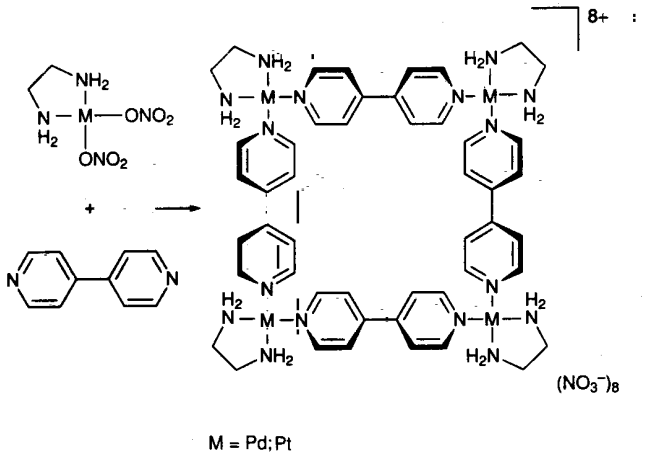

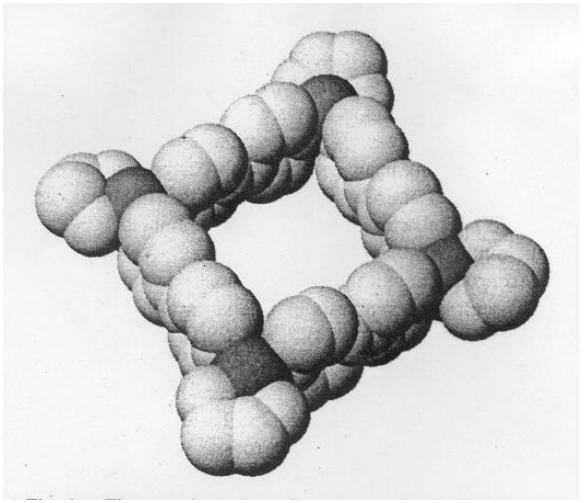

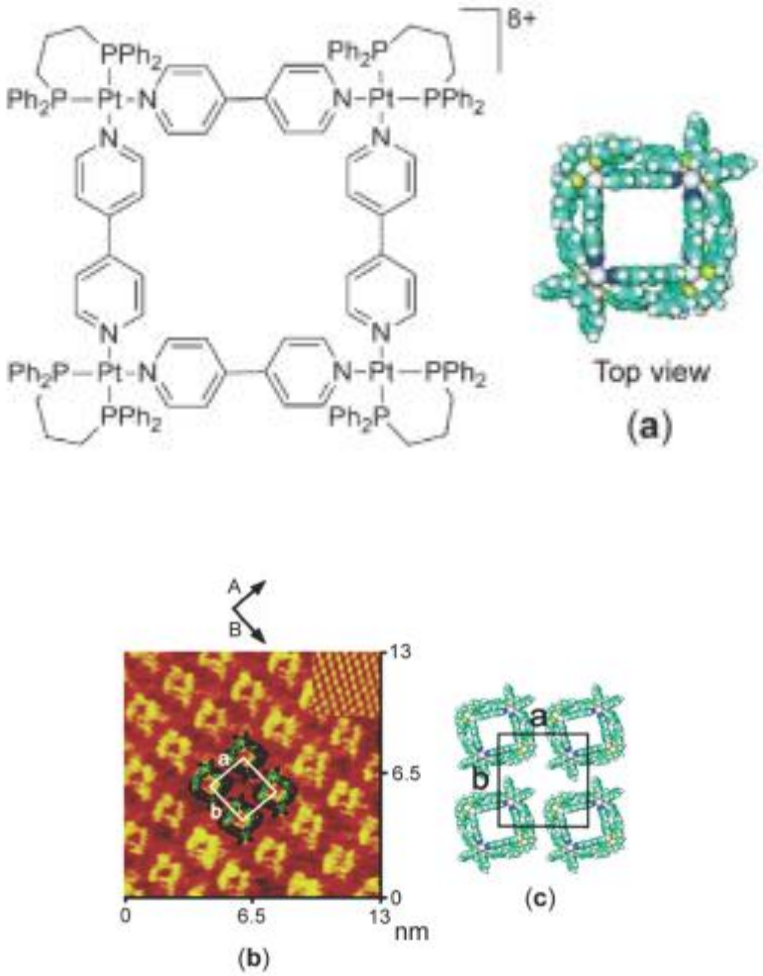

Figure 41. (a) Space-filling model of molecular square [Pt(dppp)(4,4′-bipyridine)]$_4$(PF$_6$)$_8$, (b) high-resolution STM images of the adlayer of square on Au(111), and (c) structural model of the adlayer.

Molecular Triangles

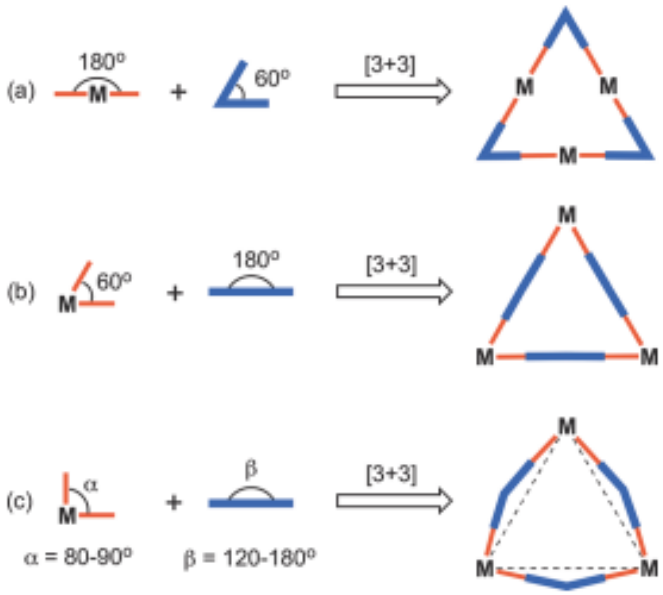

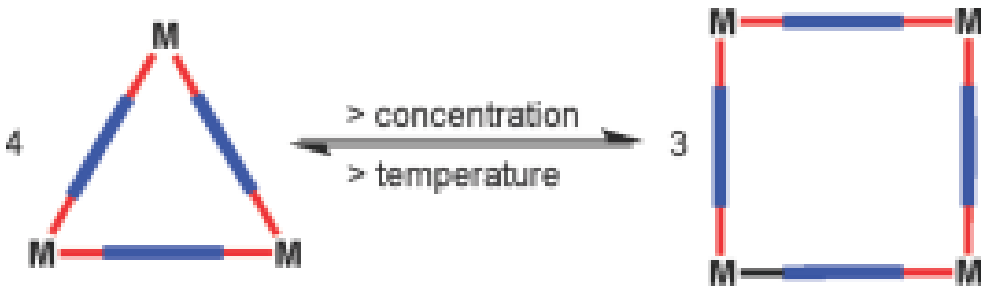

Solvent
Concentration
Temperature

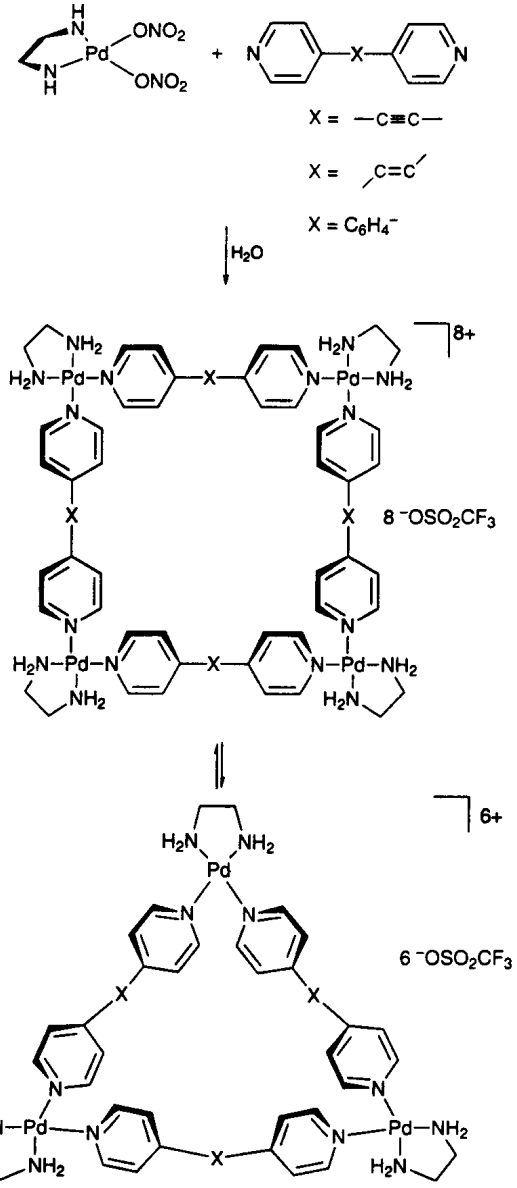
X = —C≡C—
X = C=C
X = C6H4
H2O
8+
8 −OSO2CF3
6+
6 −OSO2CF3

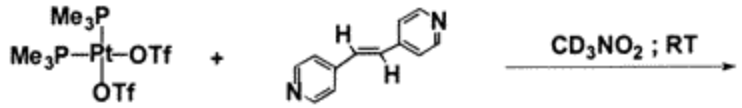

1 2

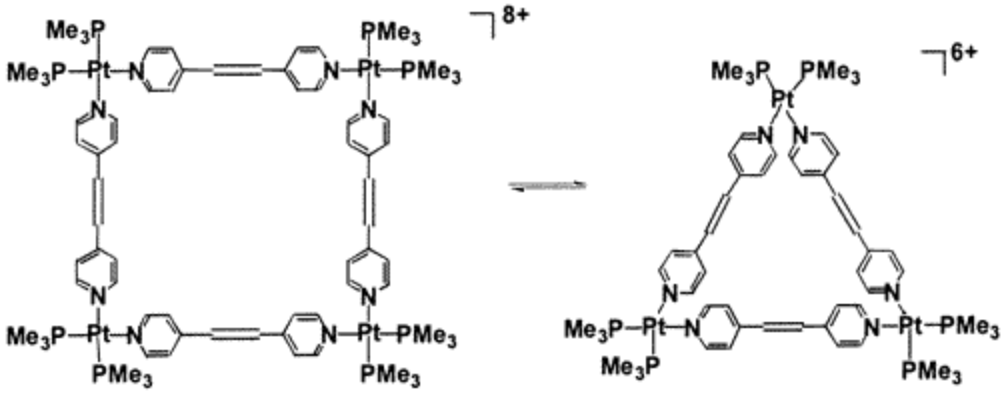

8 $CF_3SO_3^-$ 6 $CF_3SO_3^-$

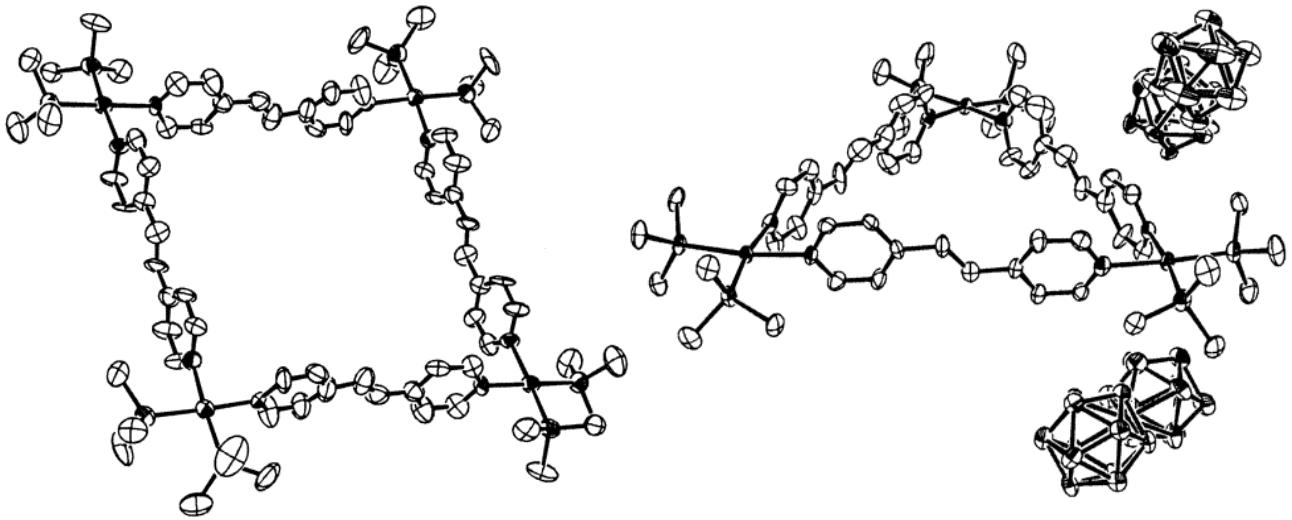

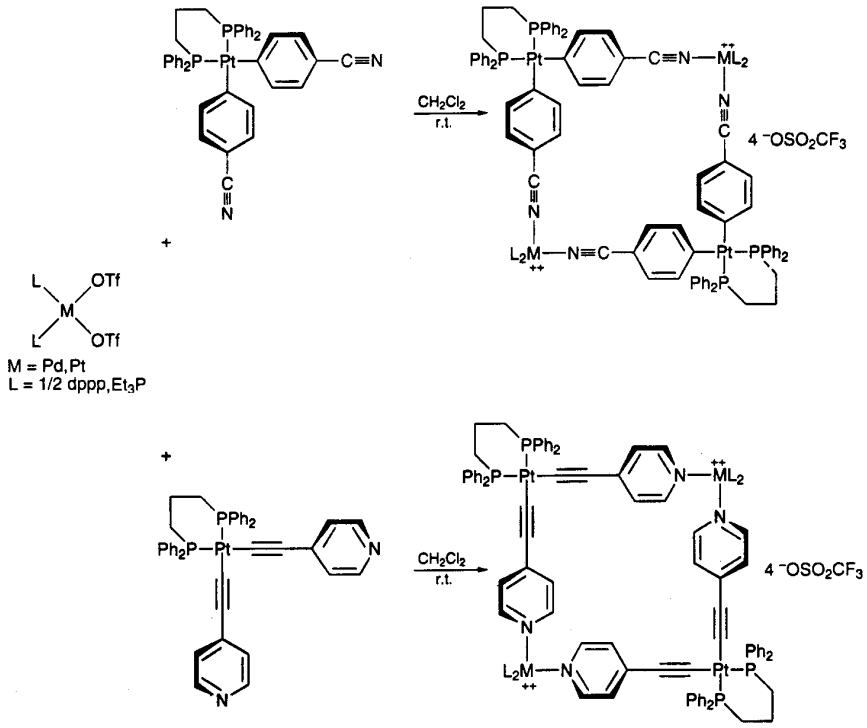
PPh2
Ph2P–Pt
C≡N
CH2Cl2
r.t.
4 −OSO2CF3
L2M
Pt–PPh2
Ph2P
L
OTf
M
L'
M = Pd,Pt
L = 1/2 dppp,Et3P
N
Ph2
P

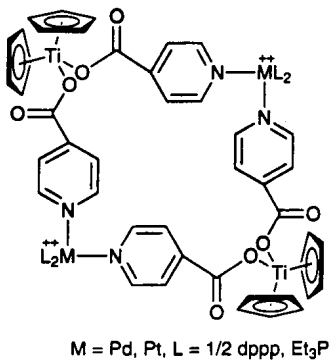
Ti
O
N
ML2
L2M
M = Pd, Pt, L = 1/2 dppp, Et3P

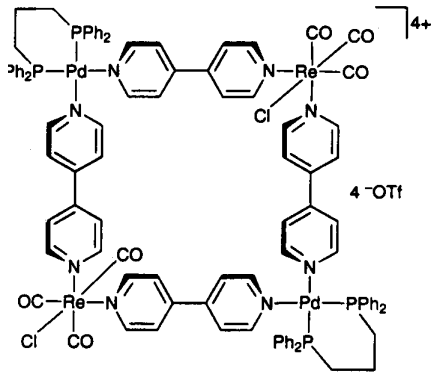
PPh2
Ph2P–Pd
CO
Re
Cl
4+
4 −OTf
OC–Re
Pd–PPh2
Ph2P

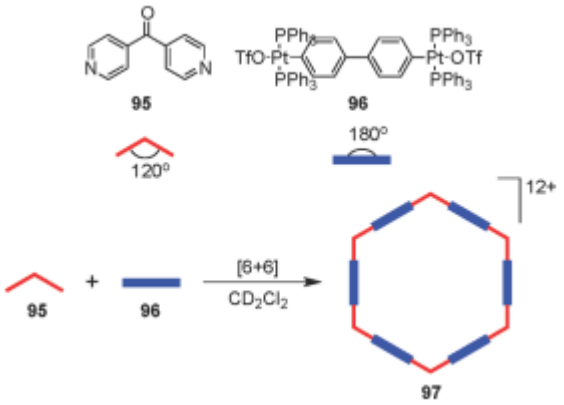
95
96
120°
180°
12+
[6+6]
CD2Cl2
97

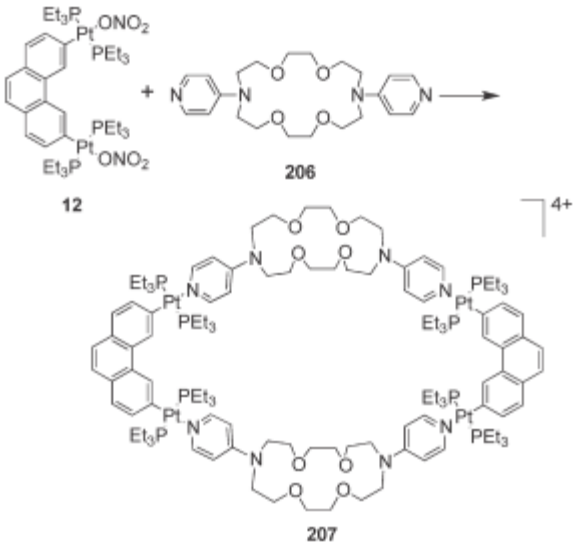
12
206
4+
207

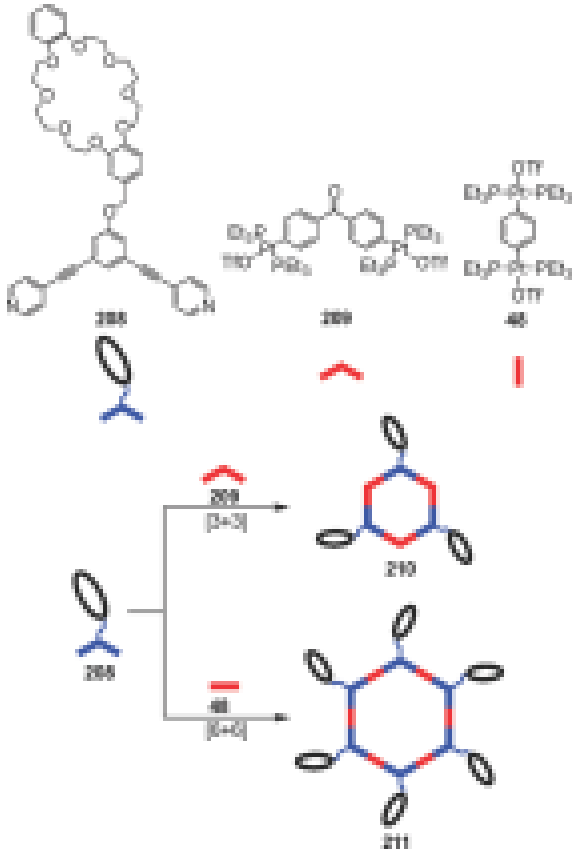
208
209
[3+3]
210
[6+6]
211

Molecular paneling *via* coordination

Chem. Commun., 2001, 509–518

Makoto Fujita,* Kazuhiko Umemoto, Michito Yoshizawa, Norifumi Fujita, Takahiro Kusukawa and Kumar Biradha

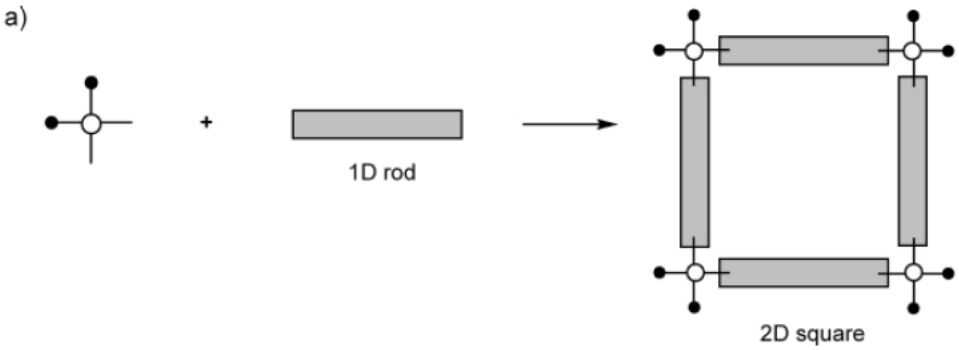

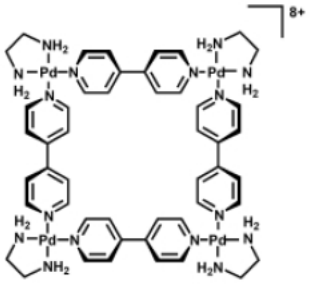

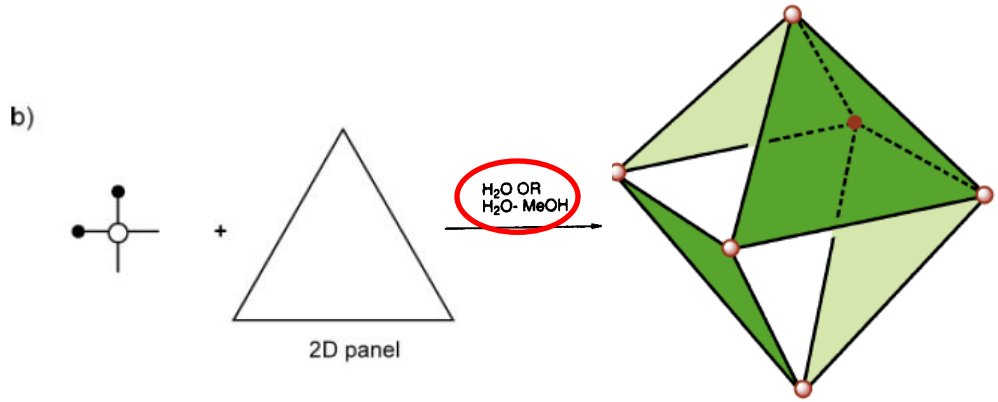

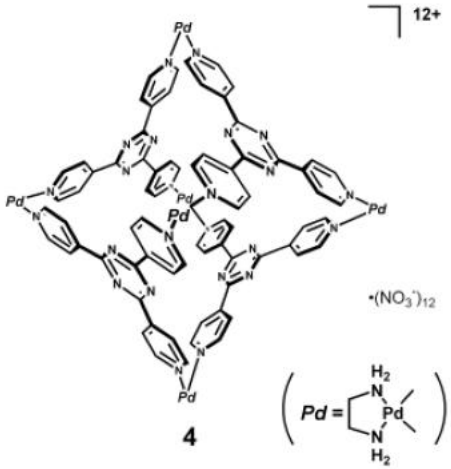

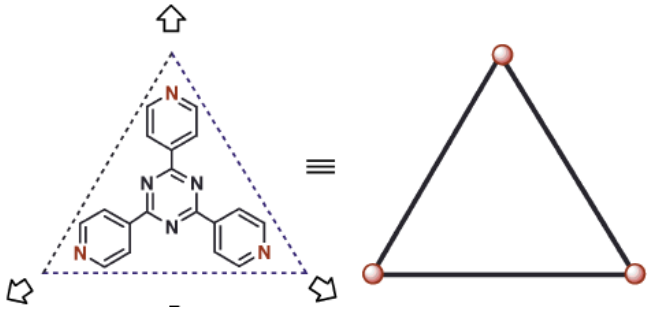

M_6L_4
d *ca.* 11 Å
Portali **8 Å**

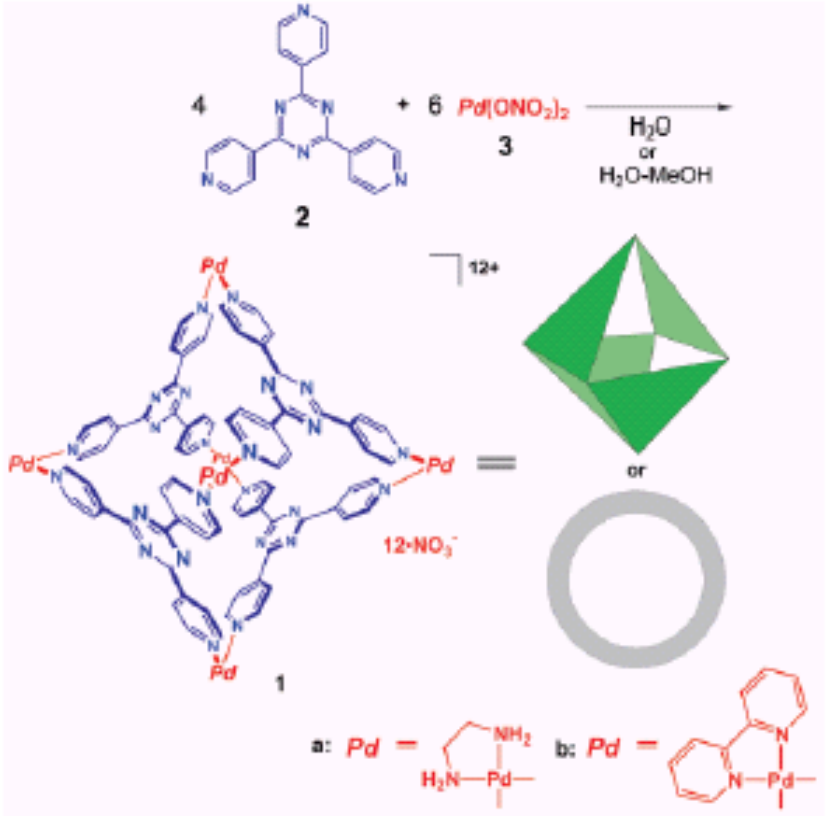
4
+ 6 Pd(ONO2)2
3
H2O
or
H2O-MeOH
2
12+
Pd
12·NO3−
or
1
a: Pd =
NH2
H2N—Pd—
b: Pd =
N
N—Pd—

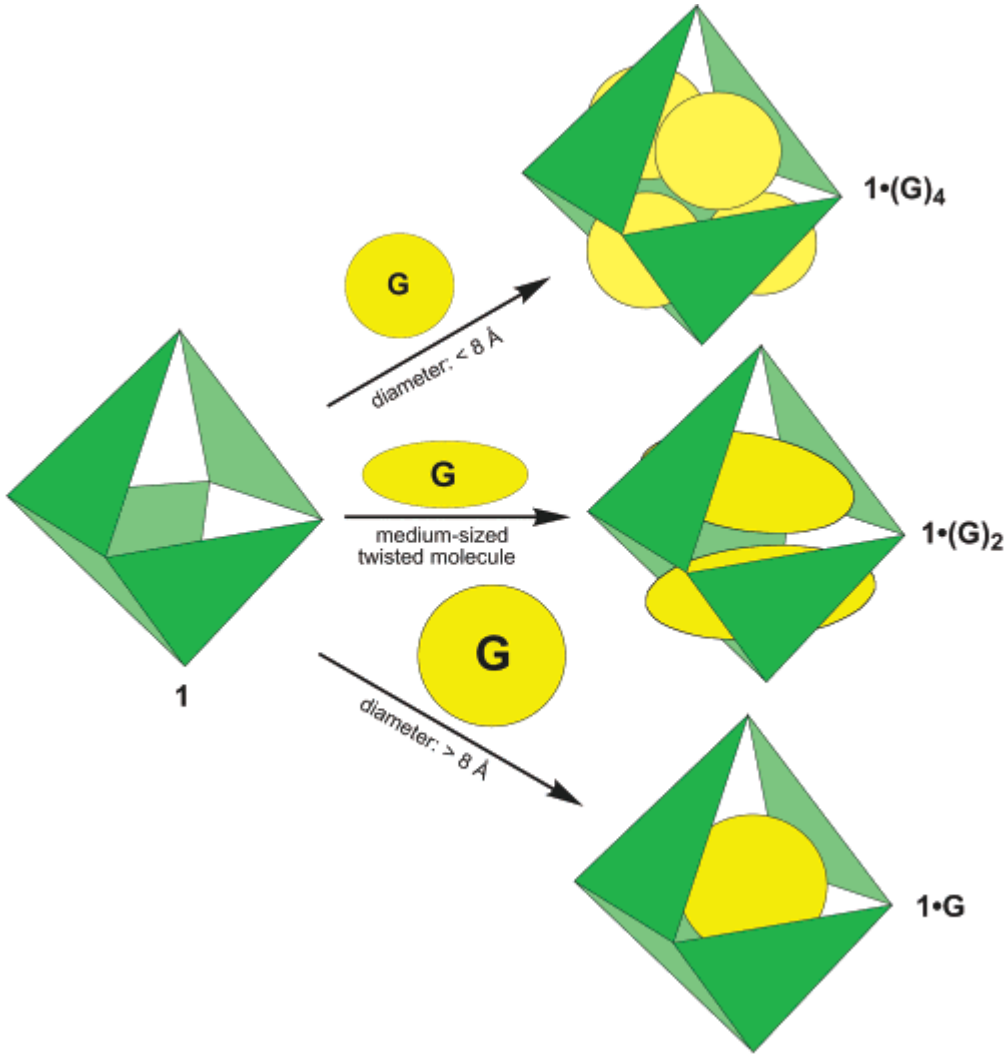
G
diameter: < 8 Å
1•(G)4
G
medium-sized
twisted molecule
1•(G)2
1
G
diameter: > 8 Å
1•G

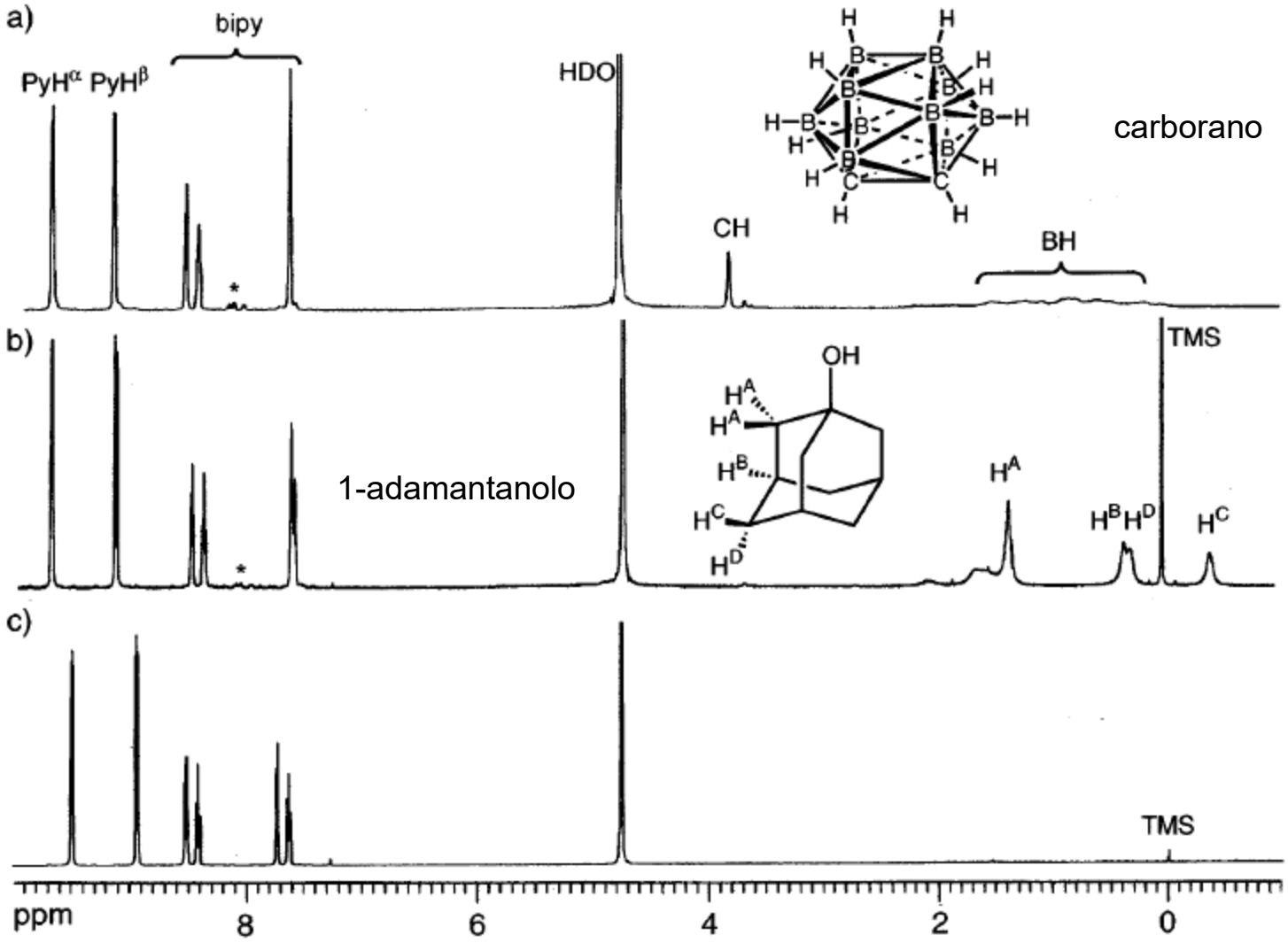

Figure 1. ^{1}H NMR observations of the enclathration of guest molecules in **1b**. (a) **1b**·(**4**)$_4$. (b) **1b**·(**5**)$_4$. (c) Empty **1b** (*: impurities).

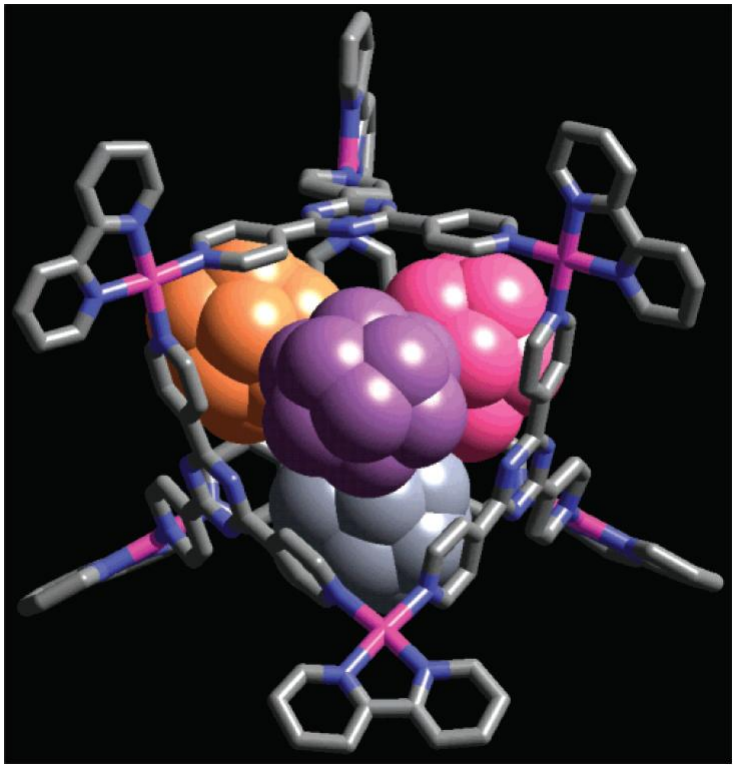

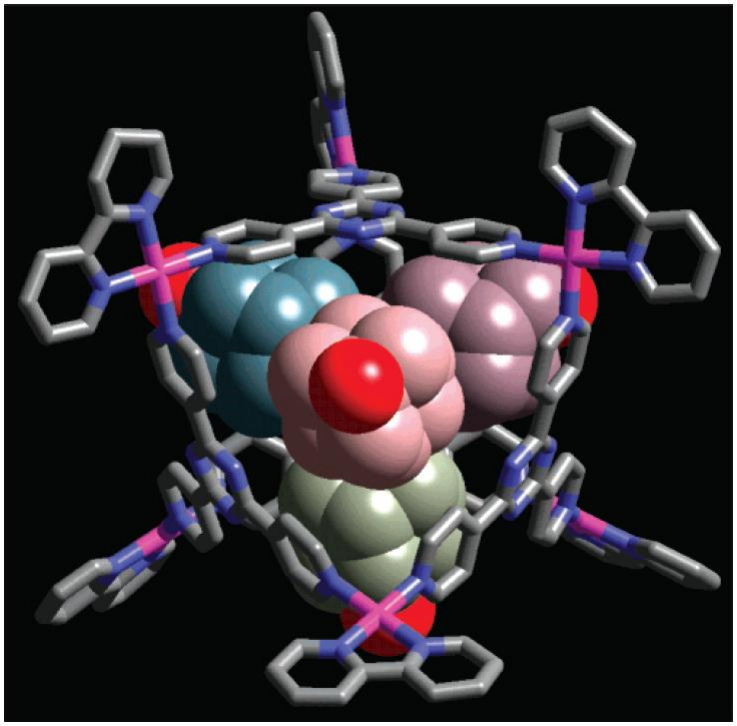

Scheme 2

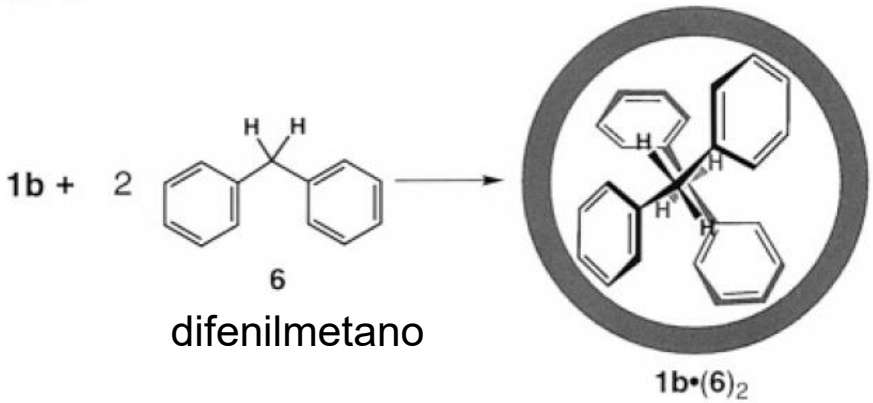

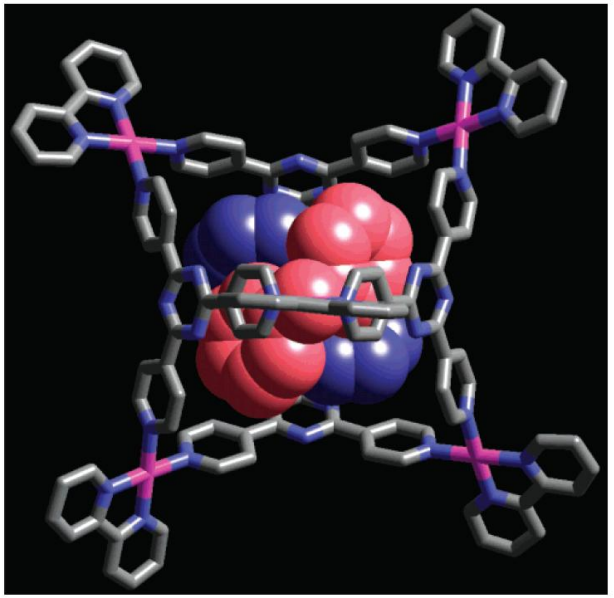

cis-azobenzene

cis-stylbene

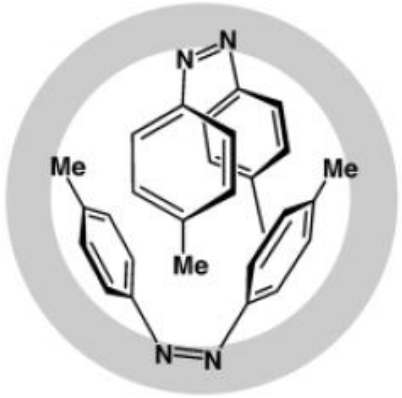

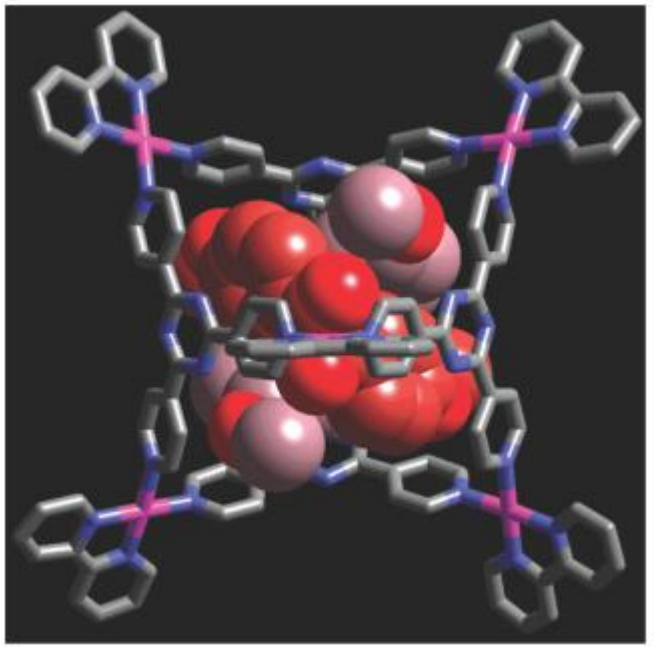

Scheme 3

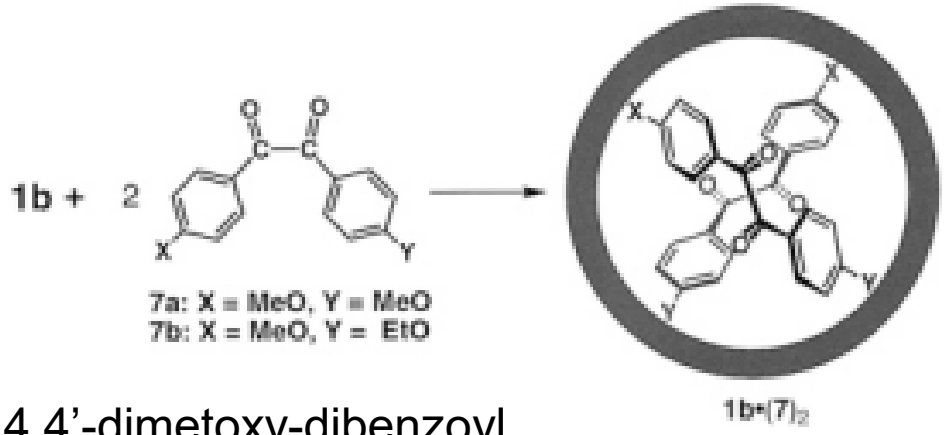

4,4’-dimetoxy-dibenzoyl

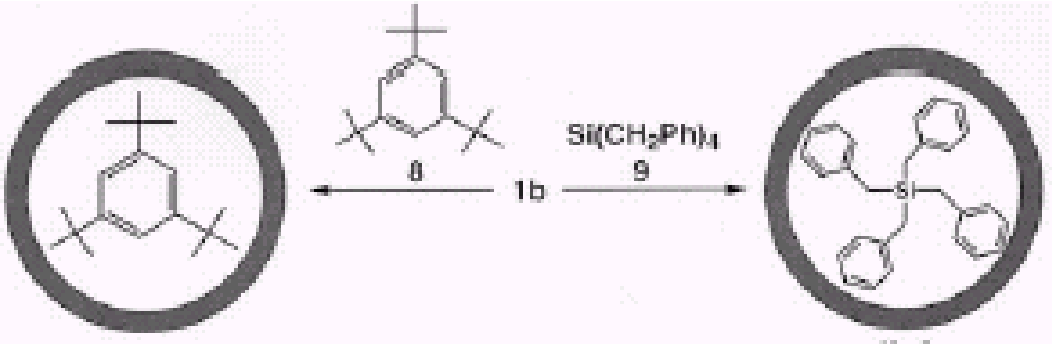

tri-*tert*-butylbenzene **tetrabenzylsilane**

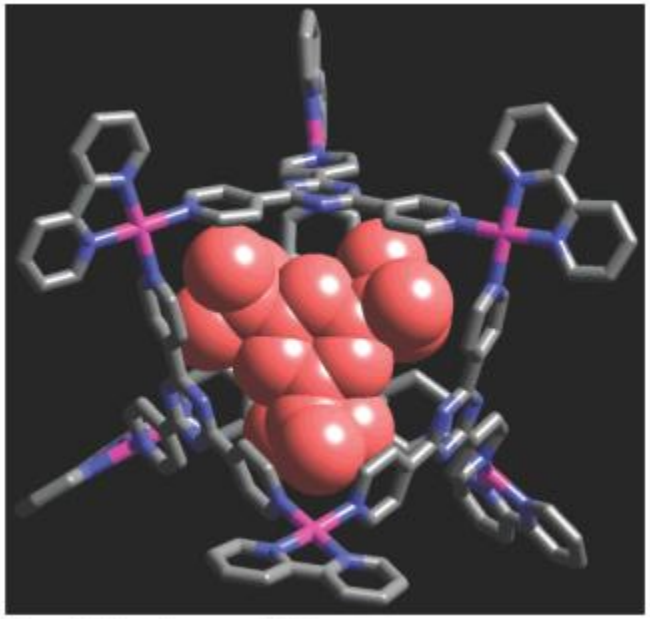

Figure 8. Crystal structure of **1b**·**8**.

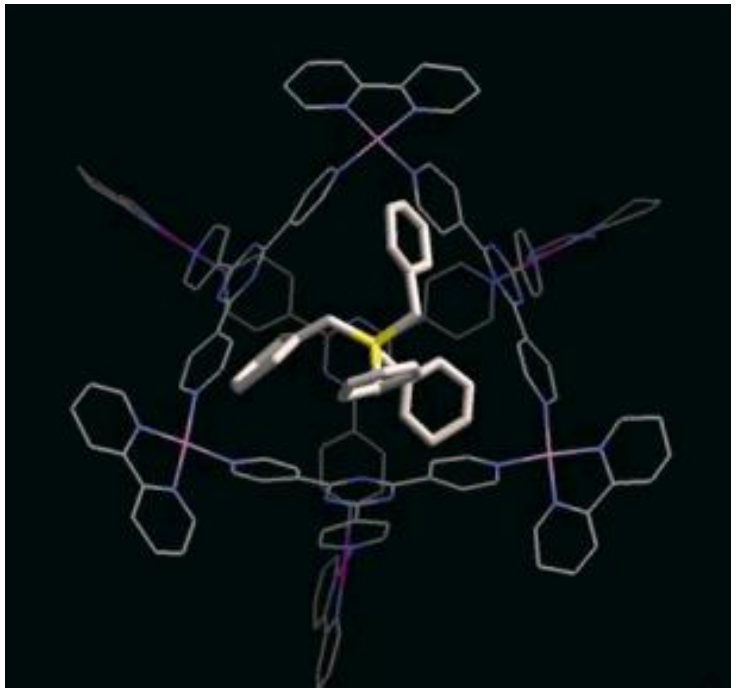

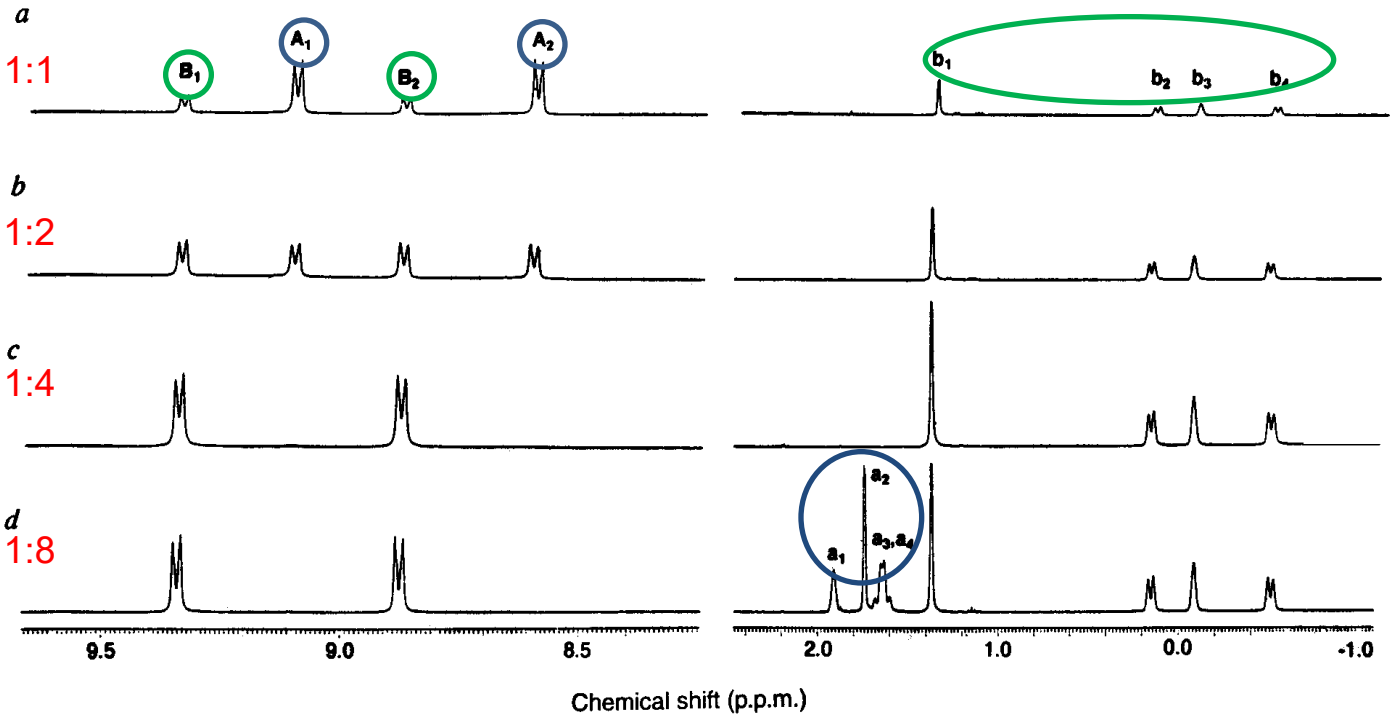

M_6L_4/adamantancarboxilate$_4$

Allosteric effect!

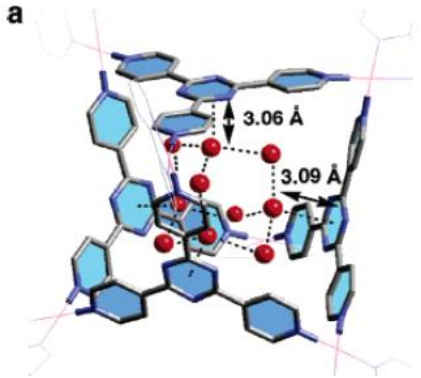

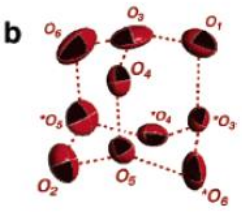

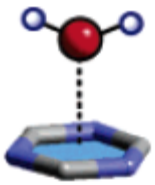

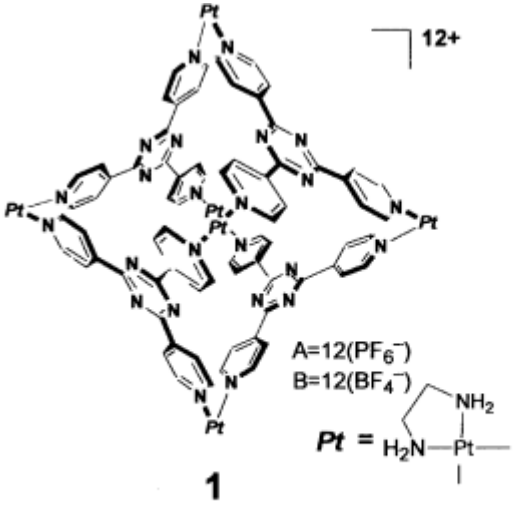

a: $(C_{84}H_{96}N_{36}Pt_6)^{12+}\cdot 12(PF_6^-)$
FW. 4519.98

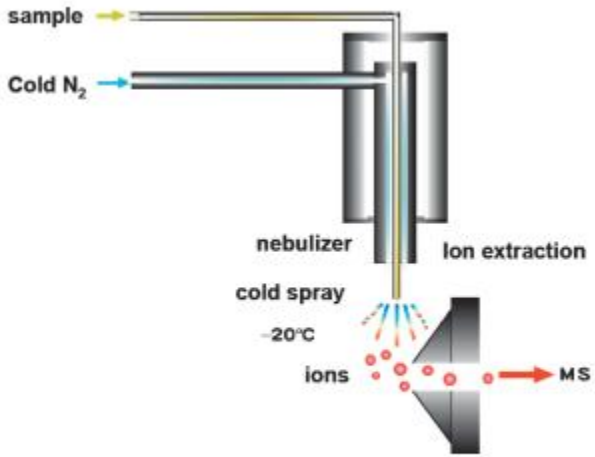

Fig. 1. Schematic illustration of the cold spray.

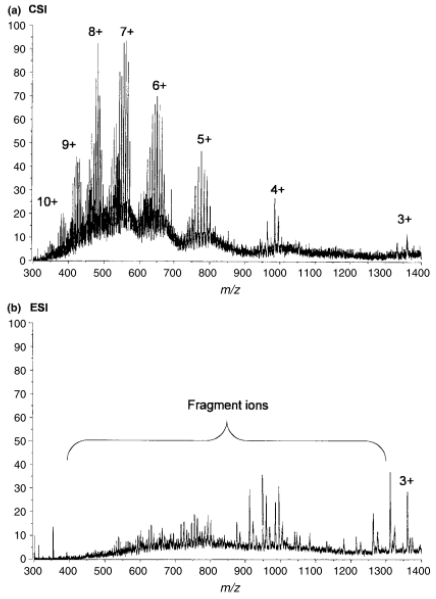

Figure 3. Comparison of (a) CSI and (b) ESI mass spectra of **1a**. Reprinted from Ref. 2 with permission from Elsevier.

Molecular Paneling

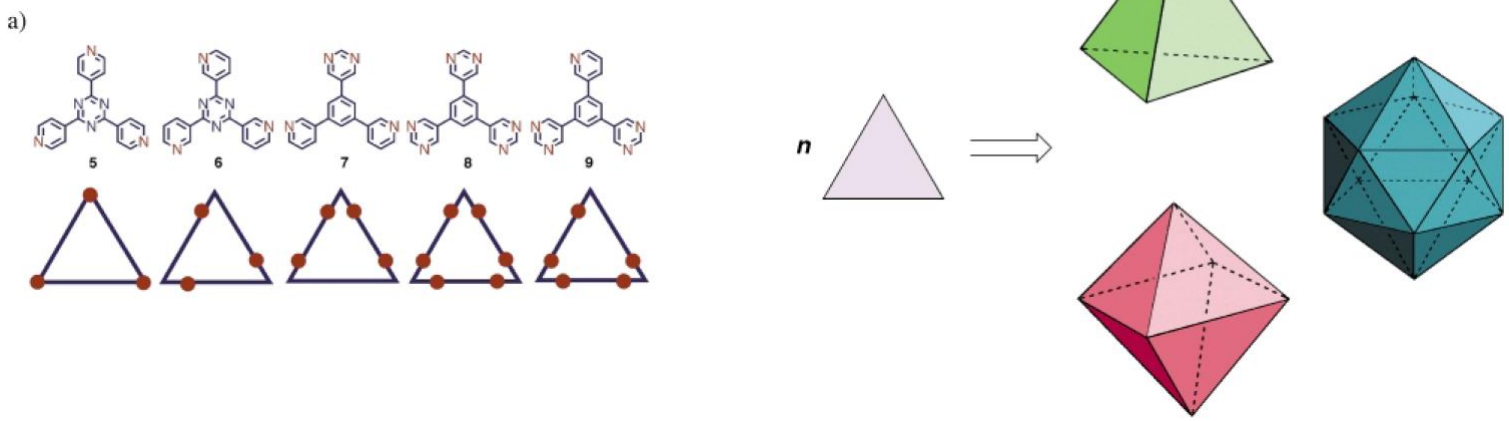

a)

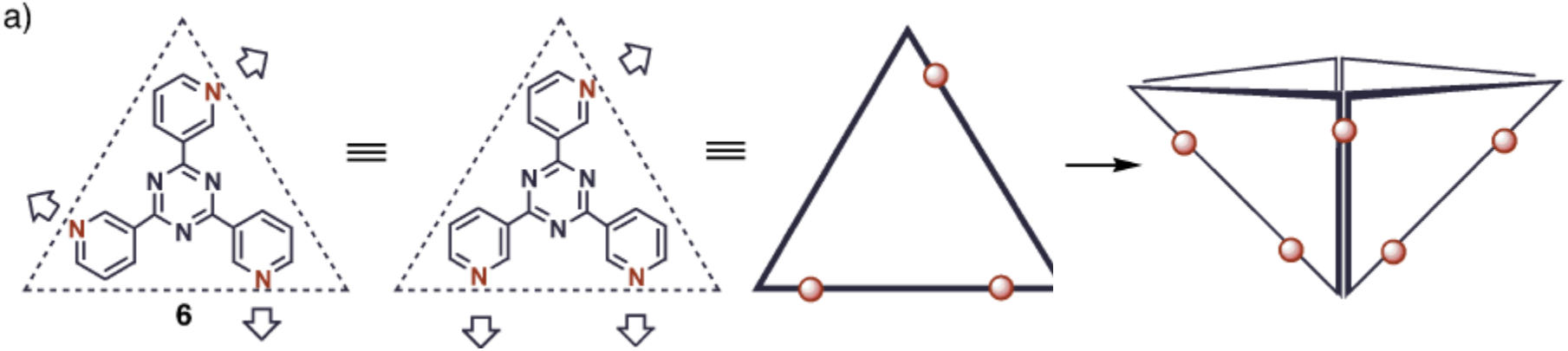

6

b)

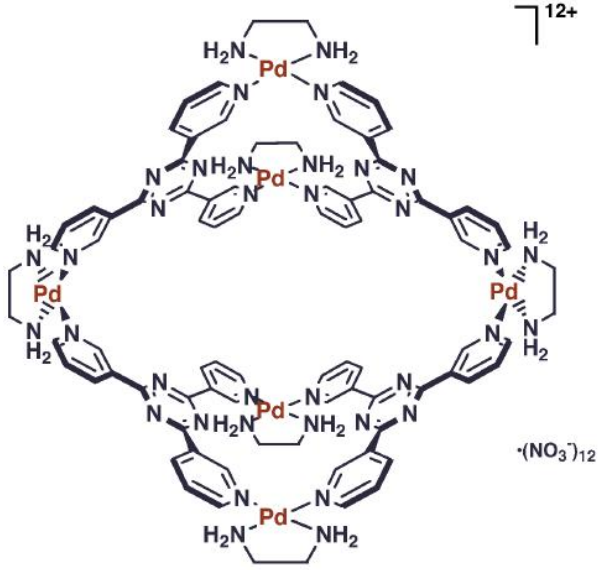

16

c)

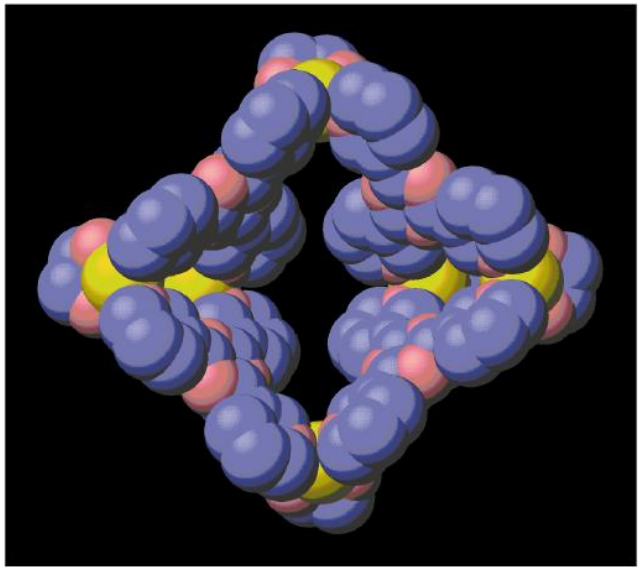

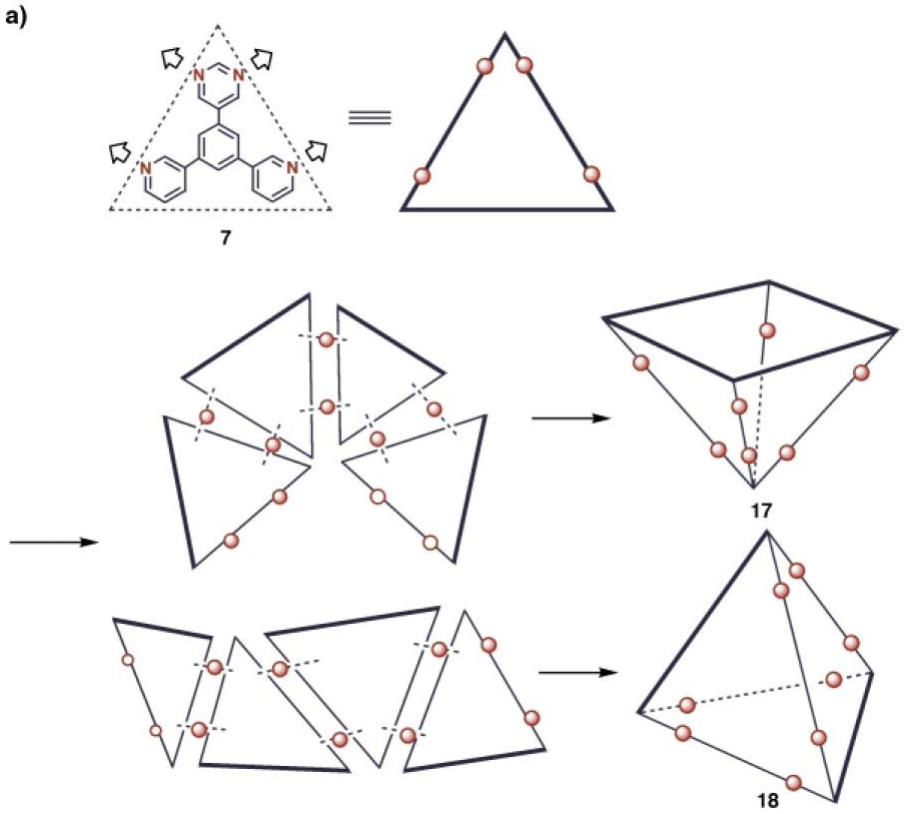
a)
N
N
N
N
7
17
18

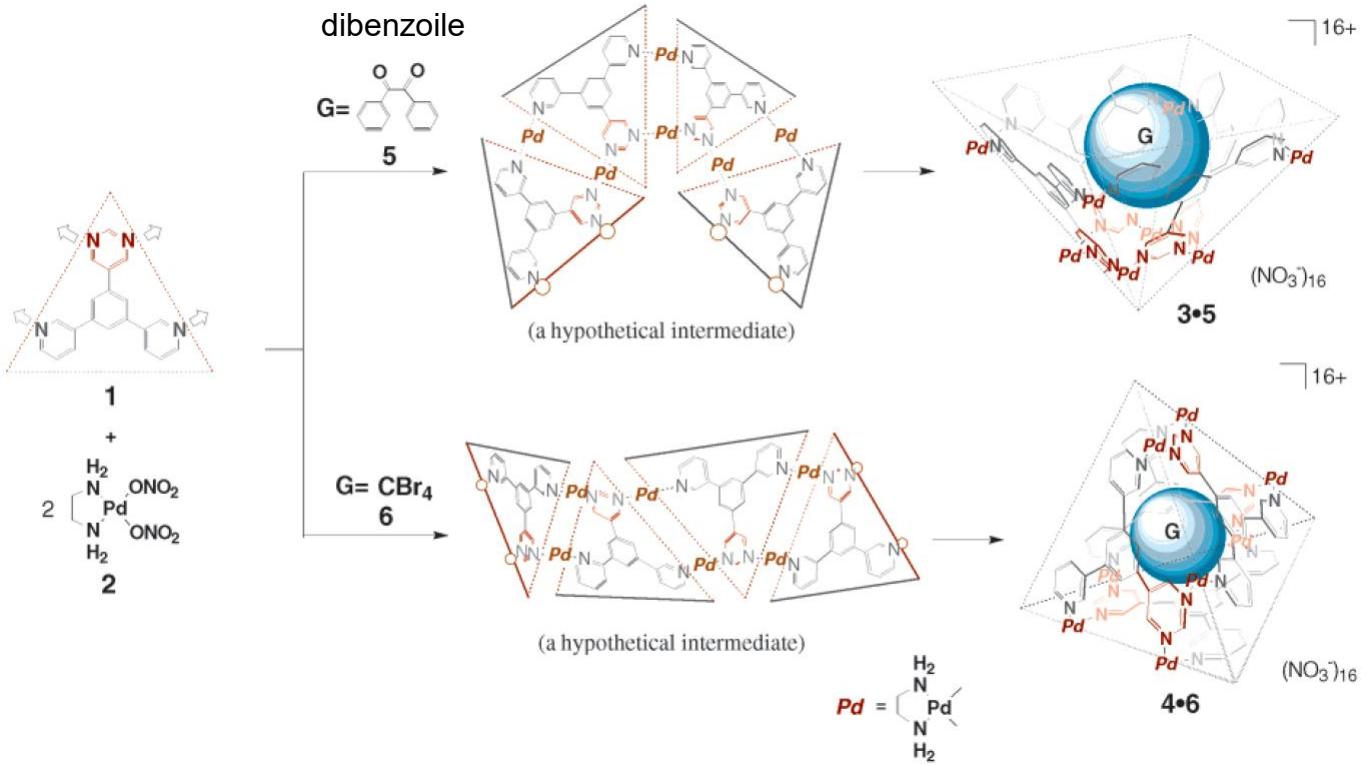
dibenzoile
G=
5
1
+
2
2
G= CBr4
6
(a hypothetical intermediate)
(a hypothetical intermediate)
16+
3•5
4•6
(NO3-)16
Pd =

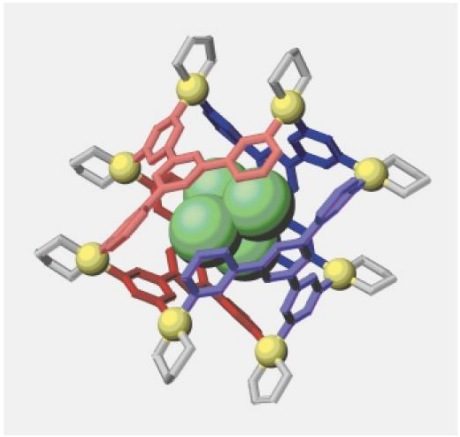

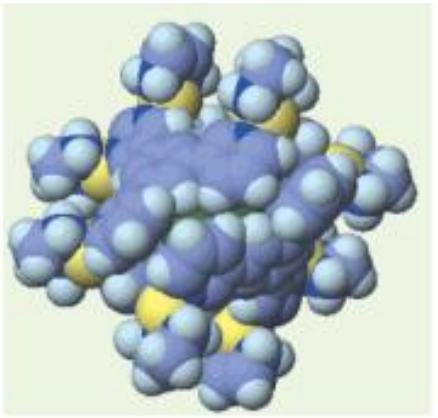

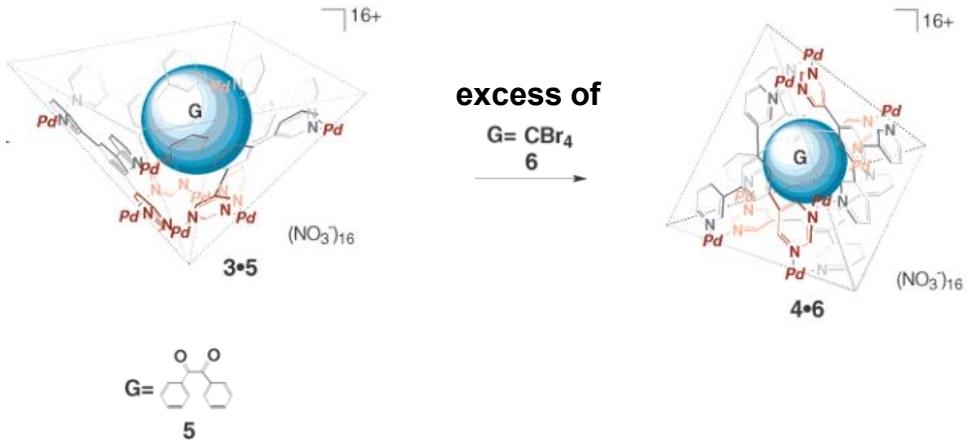
16+
3•5
(NO3-)16
excess of
G= CBr4
6
16+
4•6
(NO3-)16
G=
5

a)

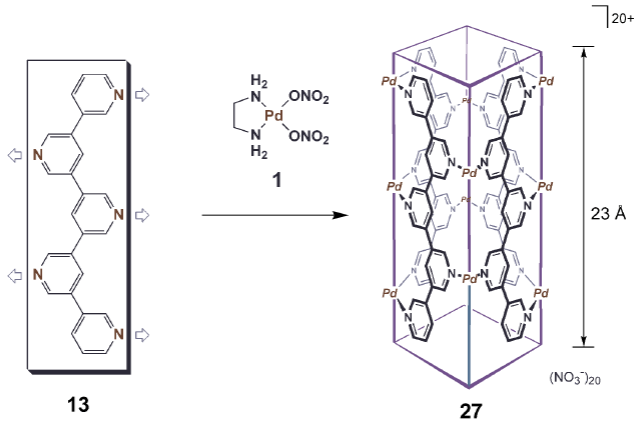
13
1
27
20+
23 Å
$(NO_3^-)_{20}$

b)

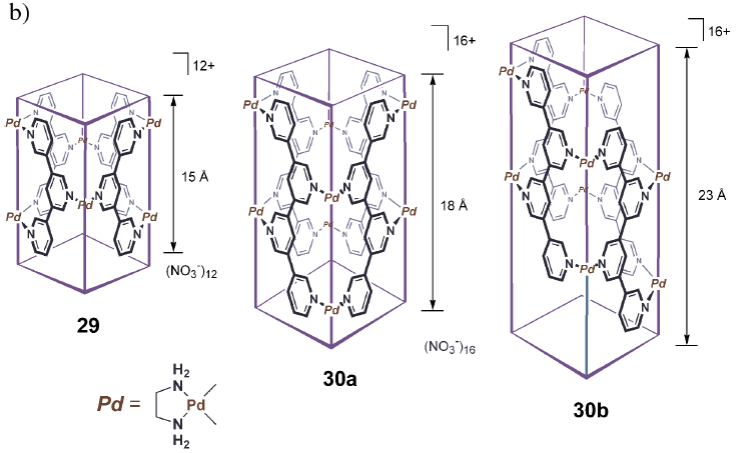
29
12+
15 Å
$(NO_3^-)_{12}$
30a
16+
18 Å
$(NO_3^-)_{16}$
30b
16+
23 Å
Pd =

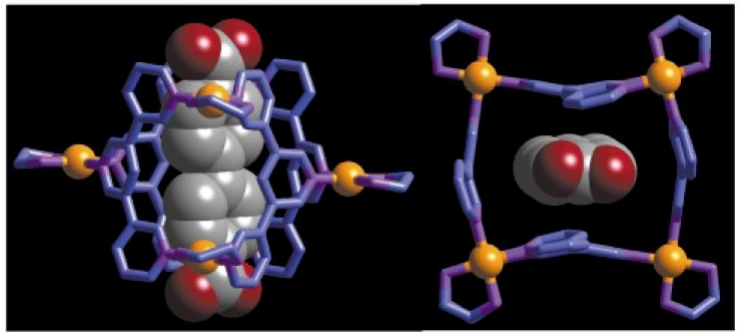

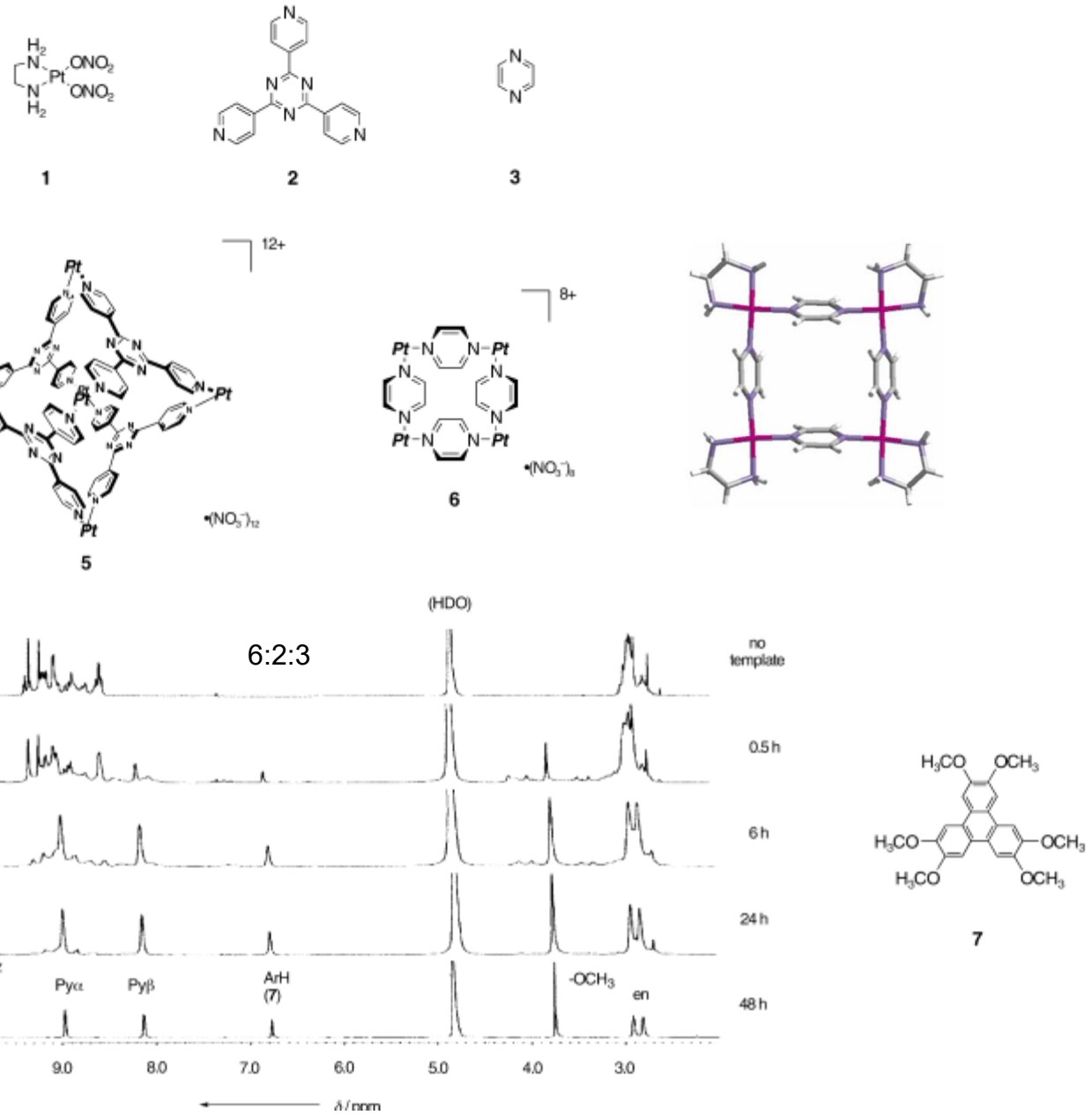

Figure 1. ^{1}H NMR spectra showing the guest-templated assembly of **7**⊂**4** complex (500 MHz, D_2O, 25 °C). a) A mixture of **1**, **2**, and **3**. Template **7** was added to this solution and the mixture was heated at 100 °C for b) 0.5 h, c) 6 h, d) 24 h, and e) 48 h. Pyz = pyrazine.

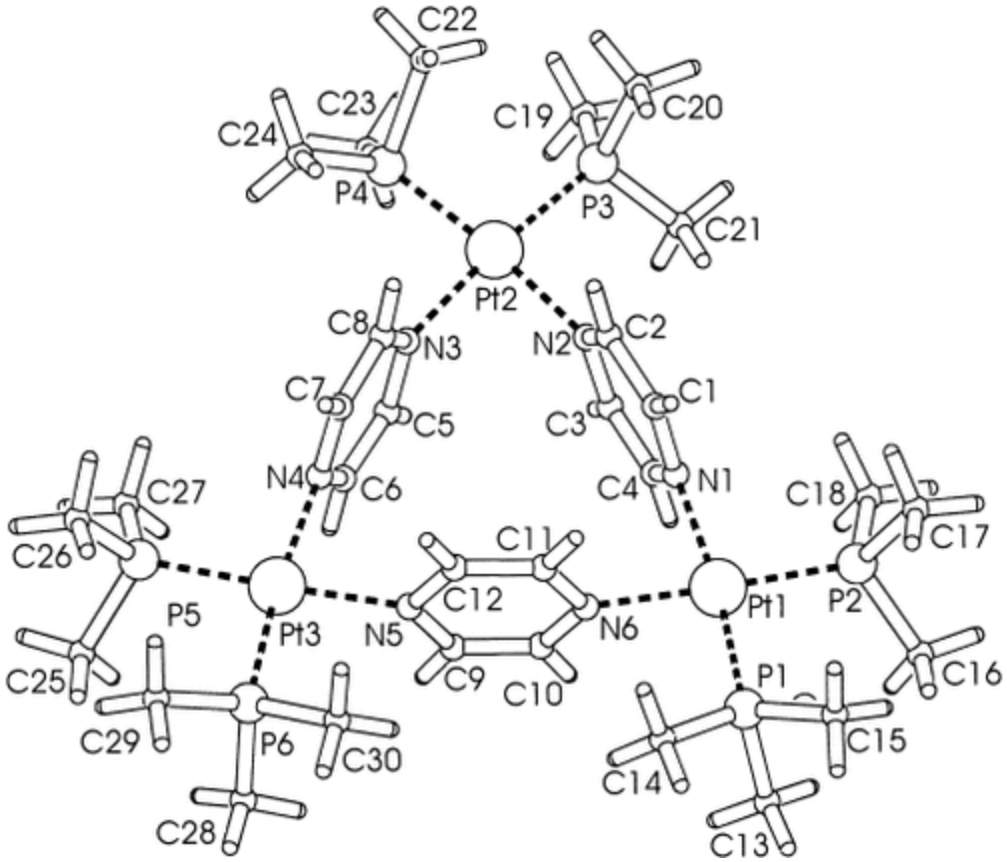
C22
C23
C24
P4
C19
C20
P3
C21
Pt2
C8
N3
N2
C2
C7
C5
C3
C1
N4
C6
C4
N1
C18
C17
C27
C26
C11
P5
Pt3
N5
C12
N6
Pt1
P2
C25
C9
C10
P1
C16
C29
P6
C30
C15
C14
C28
C13

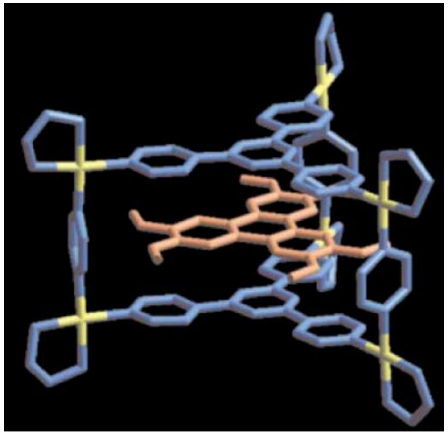

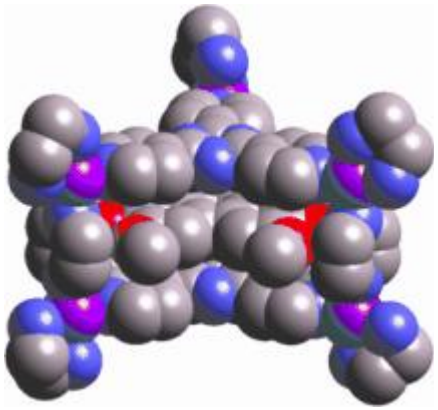

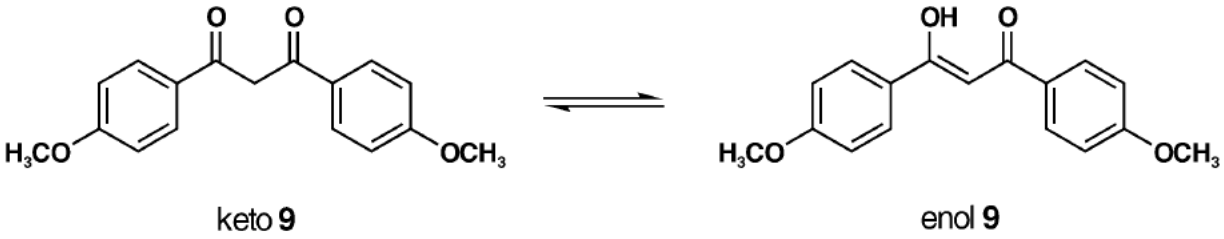

keto **9** enol **9**

The efficient intercalation of planar guest molecules within the cage was applied to the control of the equilibration between planer and nonplanar molecules. Keto and enol tautomers of β-diketone **9**, which exist in a 15:85 ratio in CD_3CN, can never be separated because of rapid tautomerization.

Stabilization of reactive intermediates: cyclic alcoxy-silanes
Ship in a Bottle

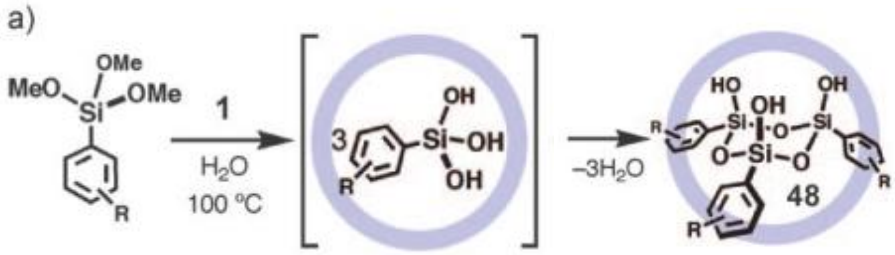

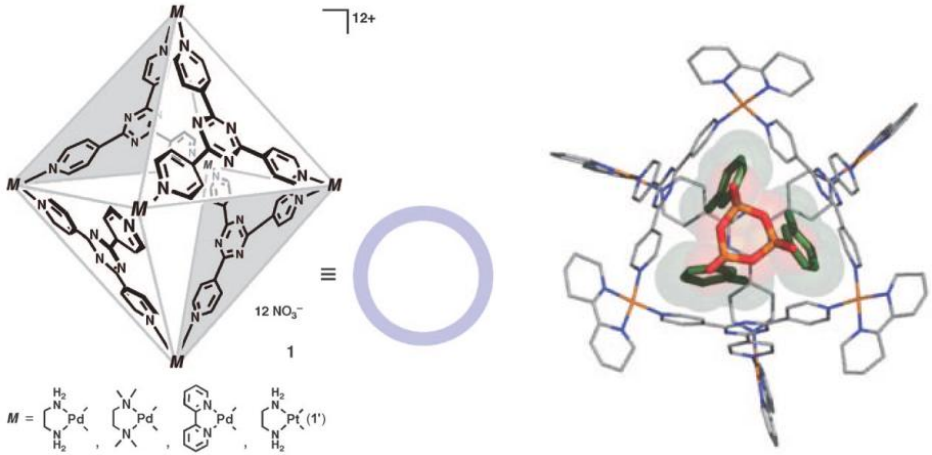

The roughly spherical cage cavity directs the selective formation of the cyclic trimer and prohibits further polycondensation despite the presence of labile Si-OH functional groups.

The stereochemistry of the condensation reaction is highly controlled within the cage giving only all-*cis* isomers.

The trimers prepared in situ can no longer escape from the cage because their dimension becomes larger than the portal size.

Stabilization of reactive intermediates: oligomerization of trialcoxy-silanes

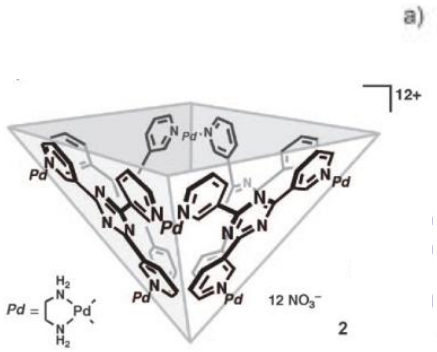

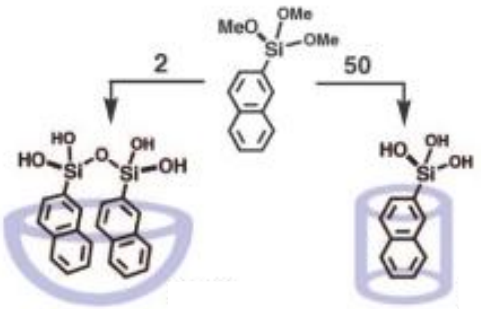

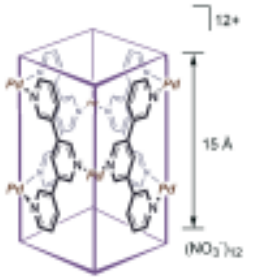

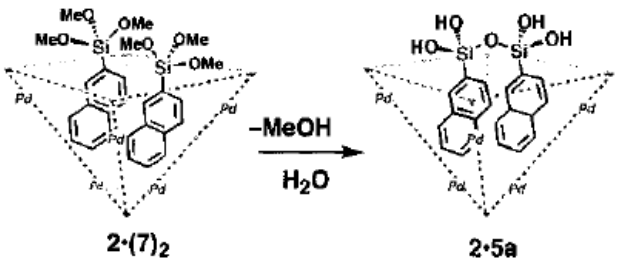

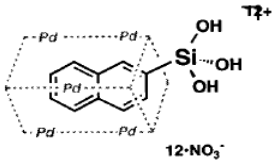

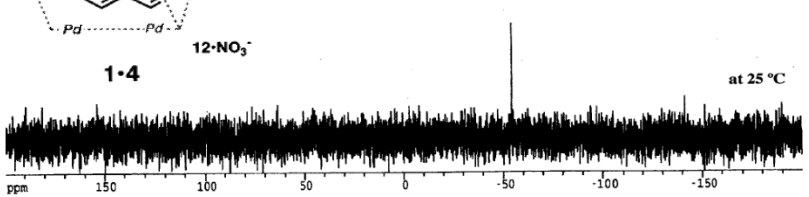

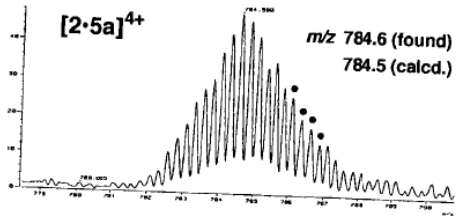

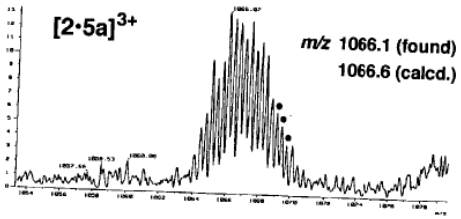

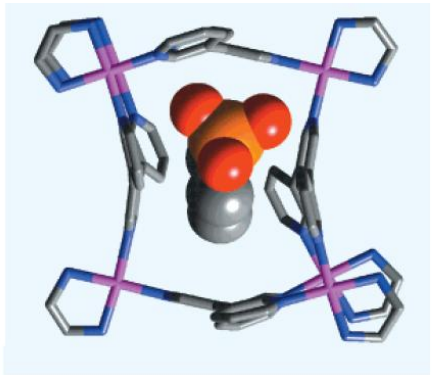

In an aqueous solution at 80 °C, the **1·4** complex remained intact for one week. Furthermore, the complex was tolerant under acidic conditions (pH <1).

Diels-Alder in Aqueous Molecular Hosts: Unusual Regioselectivity and Efficient Catalysis

Michito Yoshizawa, Masazumi Tamura, Makoto Fujita*

Science 2006;312:251-254

ERRATUM

Post date 9 June 2006

Reports: "Diels-Alder in aqueous molecular hosts: unusual regioselectivity and efficient catalysis" by M. Yoshizawa *et al.* (14 Apr. 2006, p. 251). Due to a nomenclature error, all references to "phthalimides" in the text and Supporting Online Material should instead refer to "maleimides." The chemical structures in the schemes and figures are all correct as drawn.

Fig. 1. Self-assembled coordination cages (1 and 2), which are prepared by simple mixing of an exo-tridentate organic ligand and an end-capped Pd(II) ion in a 4:6 ratio in water.

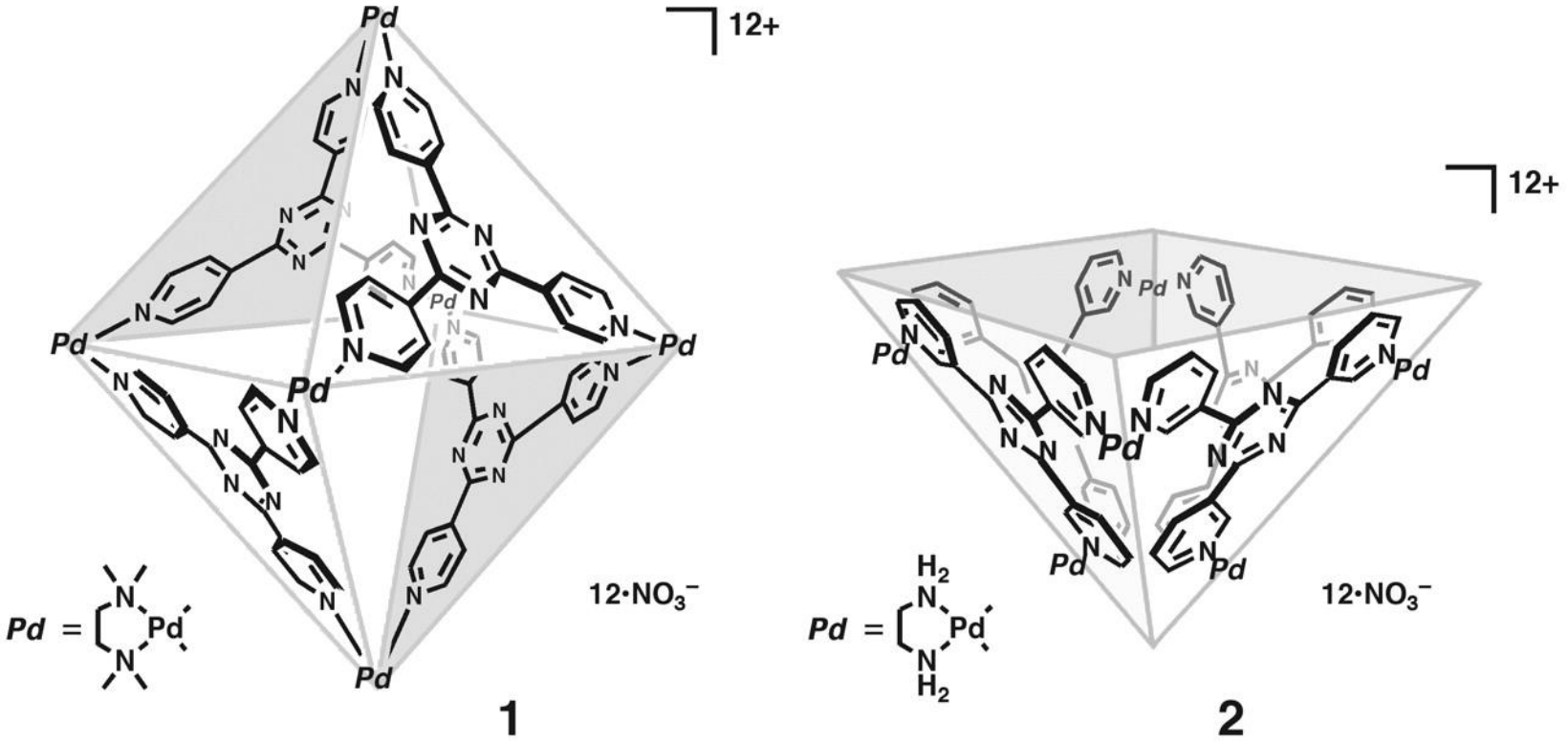

Fig. 2. (A) Pair-selective encapsulation of two types of reactants, 9-hydroxymethylanthrancene (3a) andN-cyclohexylphthalimide (4a), within cage 1 and the subsequent Diels-Alder reaction leading to syn isomer of 1,4-adduct 5 within the cavity of 1.

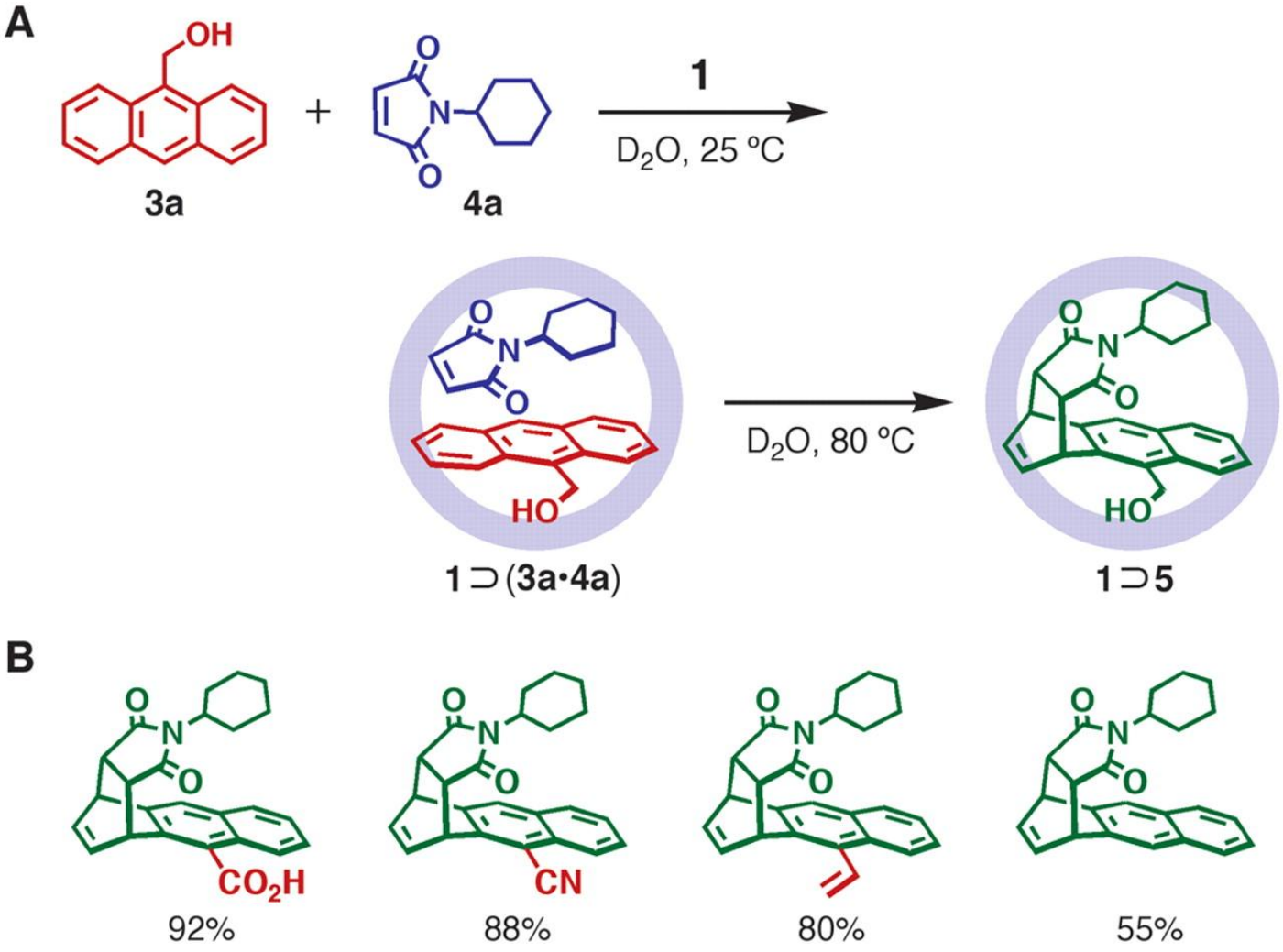

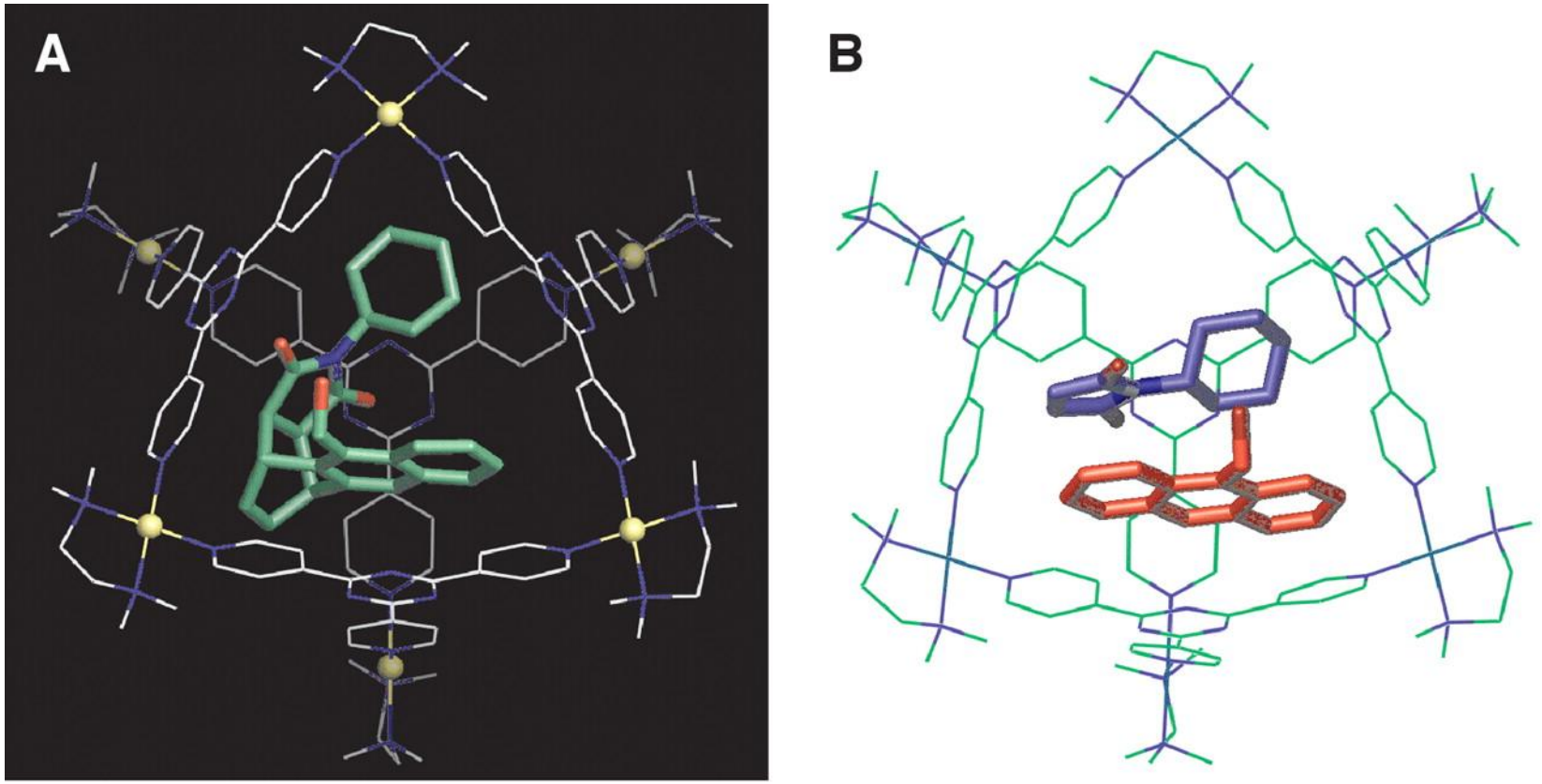
A
B

Fig. 4. Catalytic Diels-Alder reaction of 9-hydroxymethylanthracene (3a) and N-phenylphthalimide (4c) in the aqueous solution of bowl 2, leading to 9,10-adduct 6.

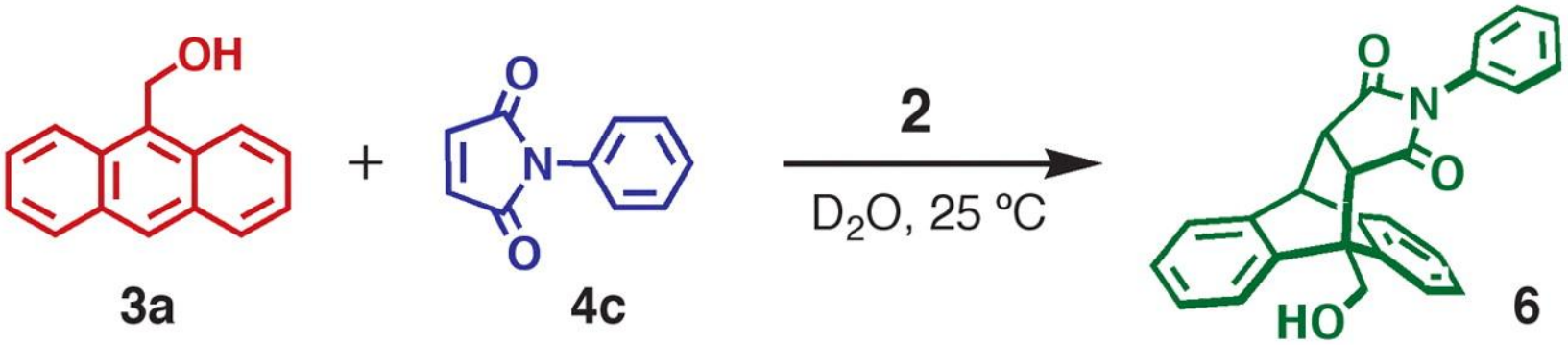

3a 4c 6

Fig. 5. The 1H NMR spectra (500 MHz, room temperature) of the catalytic Diels-Alder reaction of 9-hydroxymethylanthrancene (3a) and N-phenylphthalimide (4c) in an aqueous solution of bowl 2.

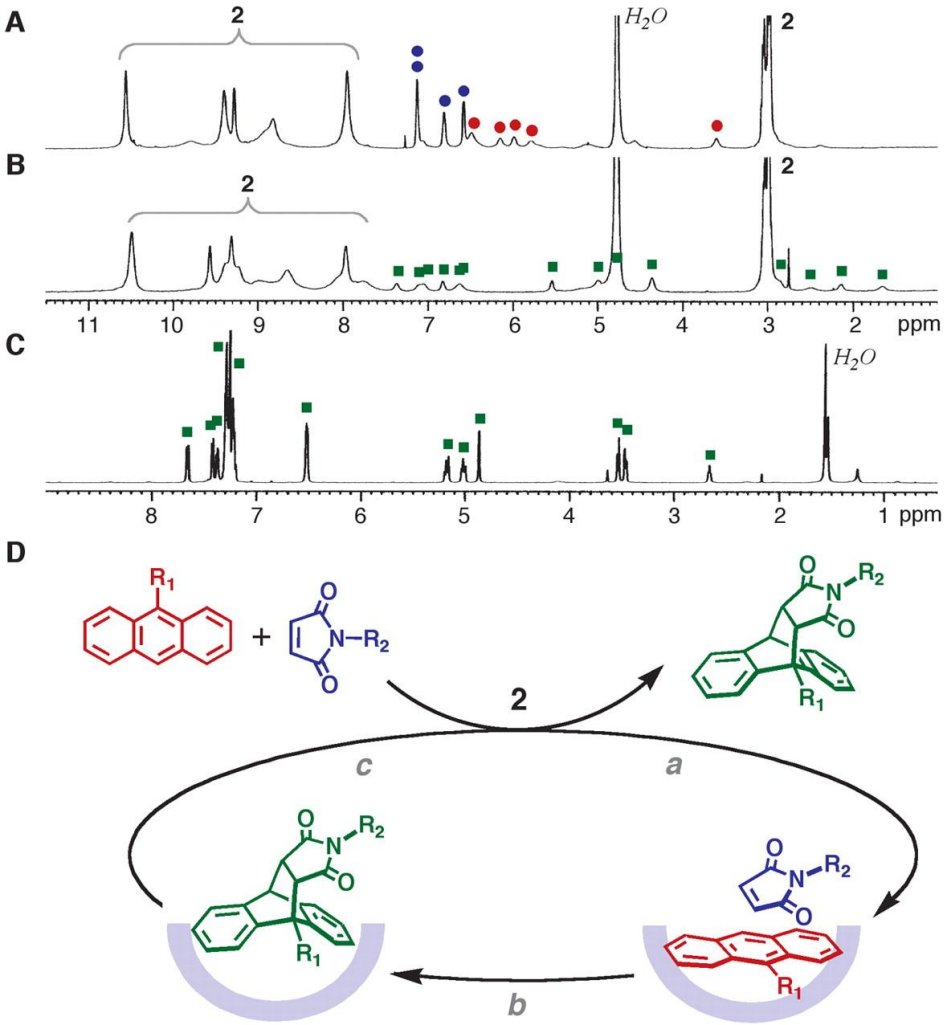

Table S1. Catalytic Diels-Alder reaction of **3** and **4** in the presence of **2** (10 mol%) in H_2O (1 mL) and control experiments in H_2O or $CDCl_3$ (1 mL) without **2**.

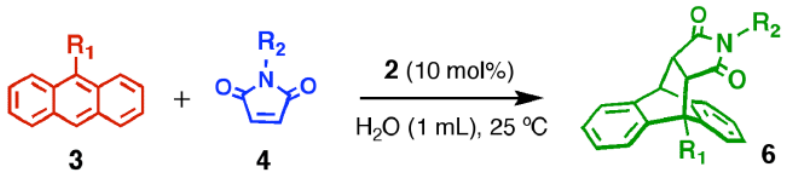

3 + **4** → **6**

Entry	Substrate		Time	Yield(%) of **6**		
	3 (R_1)	**4** (R_2)		with **2**	without **2**	in $CHCl_3$[†]
1	$-CH_2OH$	propyl	5 h	>99	8	0
2	$-CH_2OH$	cyclohexyl	15 h	98	0	6
3	$-CH_2OH$	phenyl	5 h	>99[*,†]	3	9
4	$-CH_2OH$	phenyl	15 h	6	7	21
5	$-CH_2OH$	benzyl	5 h	>99	trace	0
6	$-CH_2OH$	xylyl	15 h	94	0	17
7	$-CH_3$	cyclohexyl	7 h	>99	0	5
8	$-CH_3$	phenyl	3 h	>99	5	17
9	$-CH{=}CH_2$	phenyl	1 d	88	0	trace
10	$-CH{=}CH_2$	benzyl	1 d	97	5	4
11	$-CO_2H$	benzyl	1 d	12	0	0
12	$-CH_2OH$	phenyl	1 d	>99[‡]	—	—

[*] $(en)Pd(NO_3)_2$: 10 mol% [†] without **2** [‡] **2** : 1 mol%, hexane (1 mL)

Metal- mediated Approach:

M^{n+} as naked ions

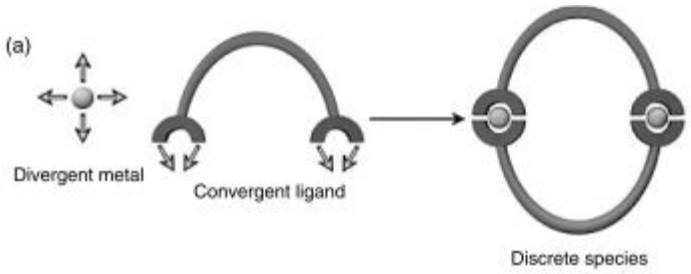

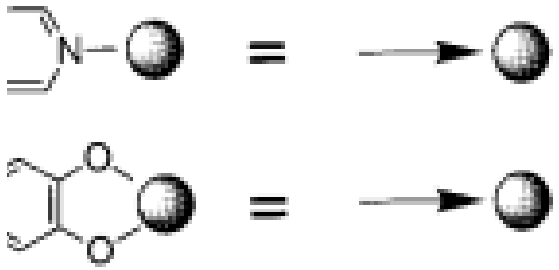

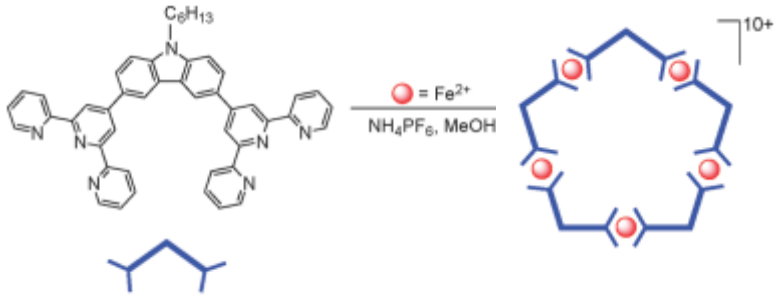

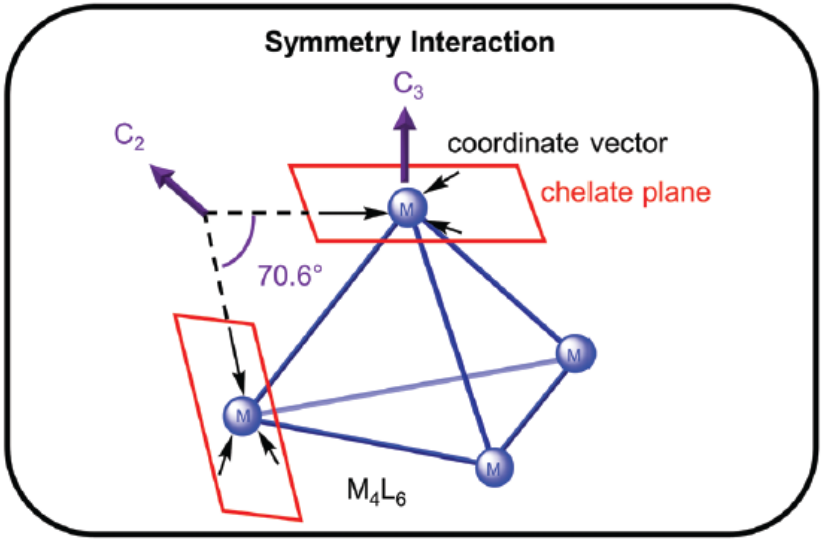

Supermolecules by Design

DANA L. CAULDER AND
KENNETH N. RAYMOND*

Acc. Chem. Res. **1999,** *32,* 975–982

J. Am. Chem. Soc. **2001,** *123,* 8923–8938

Design, Formation and Properties of Tetrahedral M_4L_4 and M_4L_6 Supramolecular Clusters[1]

Dana L. Caulder, Christian Brückner, Ryan E. Powers, Stefan König, Tatjana N. Parac, Julie A. Leary, and Kenneth N. Raymond*

In the symmetry interaction approach, Raymond and co-workers defined the symmetry of the cage in terms of the geometric relationship between the metal and ligand, as represented by the coordinate vector (from the interaction between the metal and ligand) and chelate plane (defined by the plane in which the coordinate vectors of the chelating ligands lie). For a M_4L_6 tetrahedron, the three coordinate vectors of each metal complex form a chelate plane containing a C_3 axis and an angle of 70.6° is required between the coordinate vectors within each ligand to bridge the metal centres.

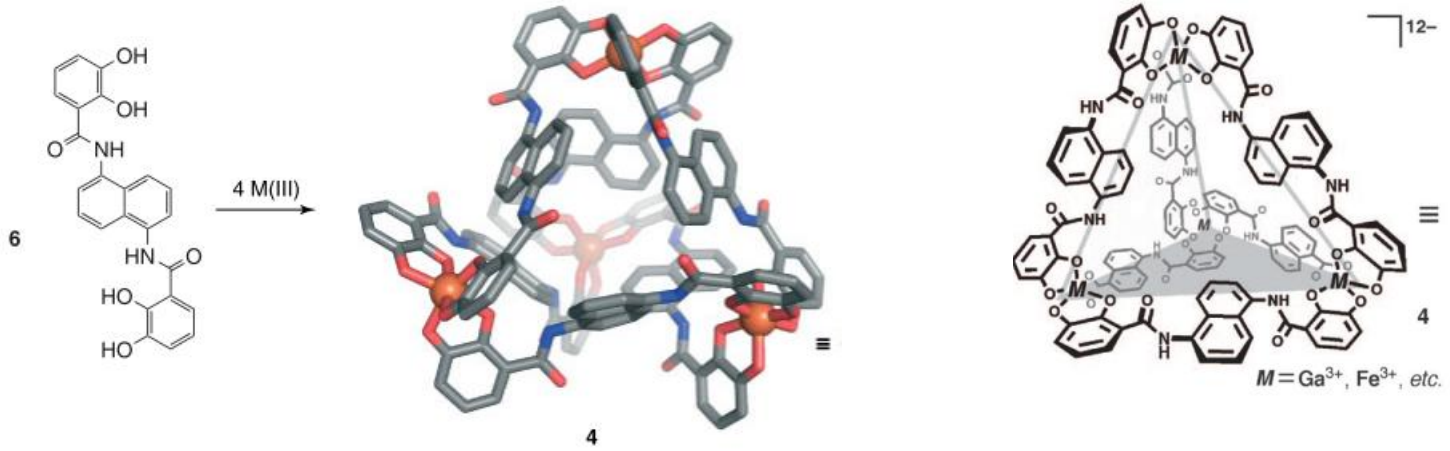

M_4L_6, (Ga^{3+}, Fe^{3+}; biscatechol-amides) **12**$^{-}$, ΔΔΔΔ, ΛΛΛΛ, 300-350 Å
Stabilization of organic cations

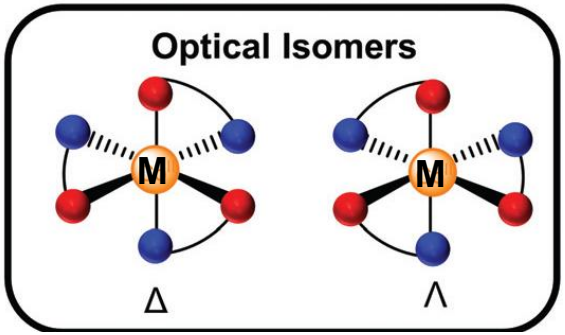

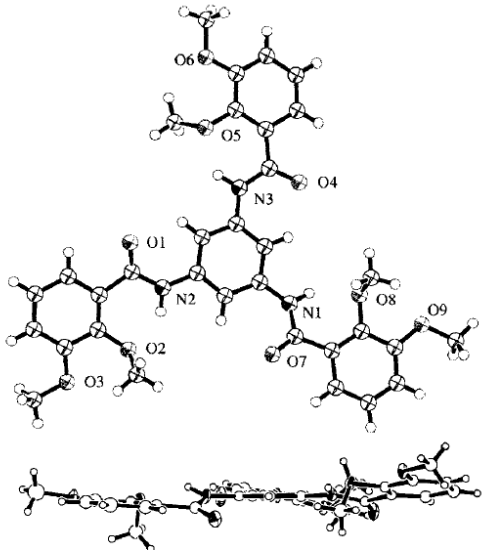

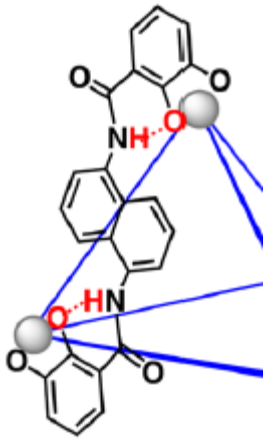

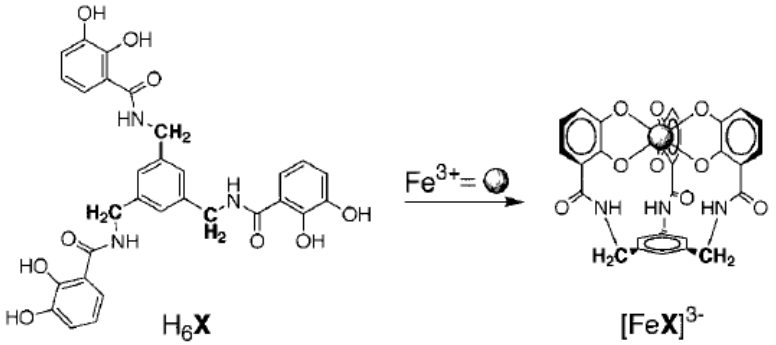

Figure 4. As shown in the enterobactin analogue H_6**X**, simple addition of a methylene group between the three-fold benzene scaffold and the catecholamide binding units gives the ligand enough flexibility to allow each of the arms to coordinate a single metal ion. This type of ligand flexibility must be avoided if multimetal clusters are desired.

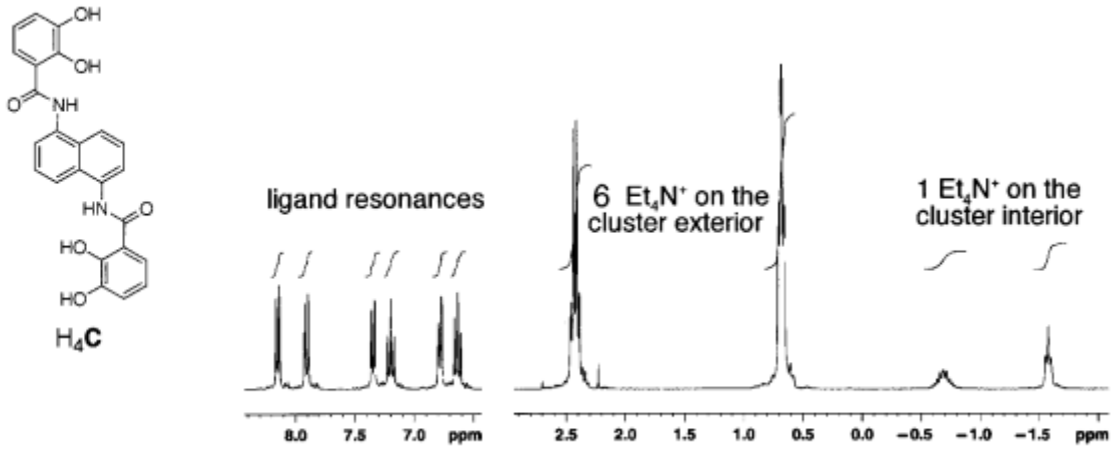

Figure 14. ^{1}H NMR (D_2O) depicting the two sets of Et_4N^+ resonances characteristic of the exterior and encapsulated cations.

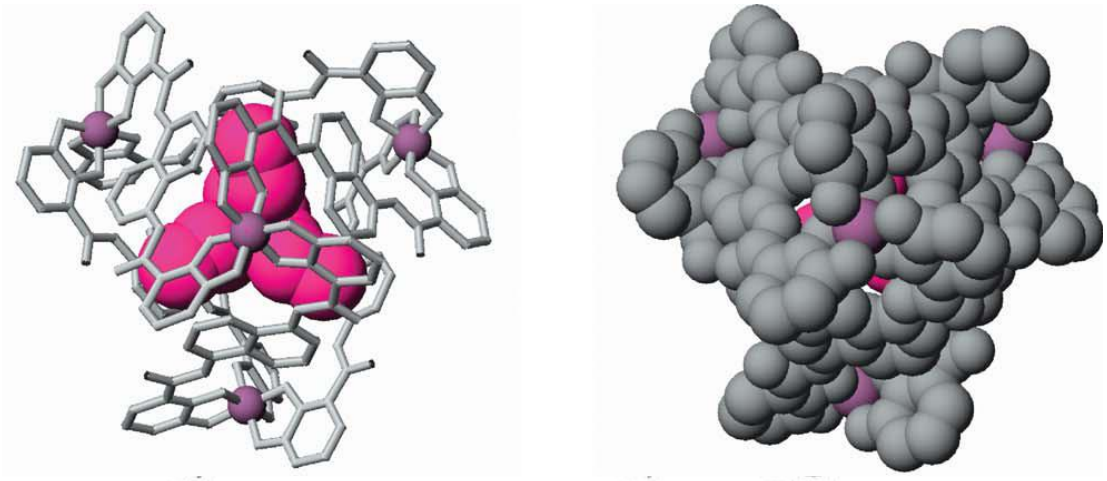

Figure 15. Based on the X-ray structure coordinates, $Et_4N^+ \subset [Fe_4C_6]^{12-}$ in both (a) wire-frame and (b) space-filling representations.

ESI-MS data

Guest exchange in an M_4L_6 supramolecular host has been evaluated to determine whether host rupture is required for guest ingress and egress. Two mechanistic models were evaluated: one requiring partial dissociation of the host structure to create a portal for guest passage and one necessitating deformation of the host structure to create a dilated aperture for guest passage without host rupture.

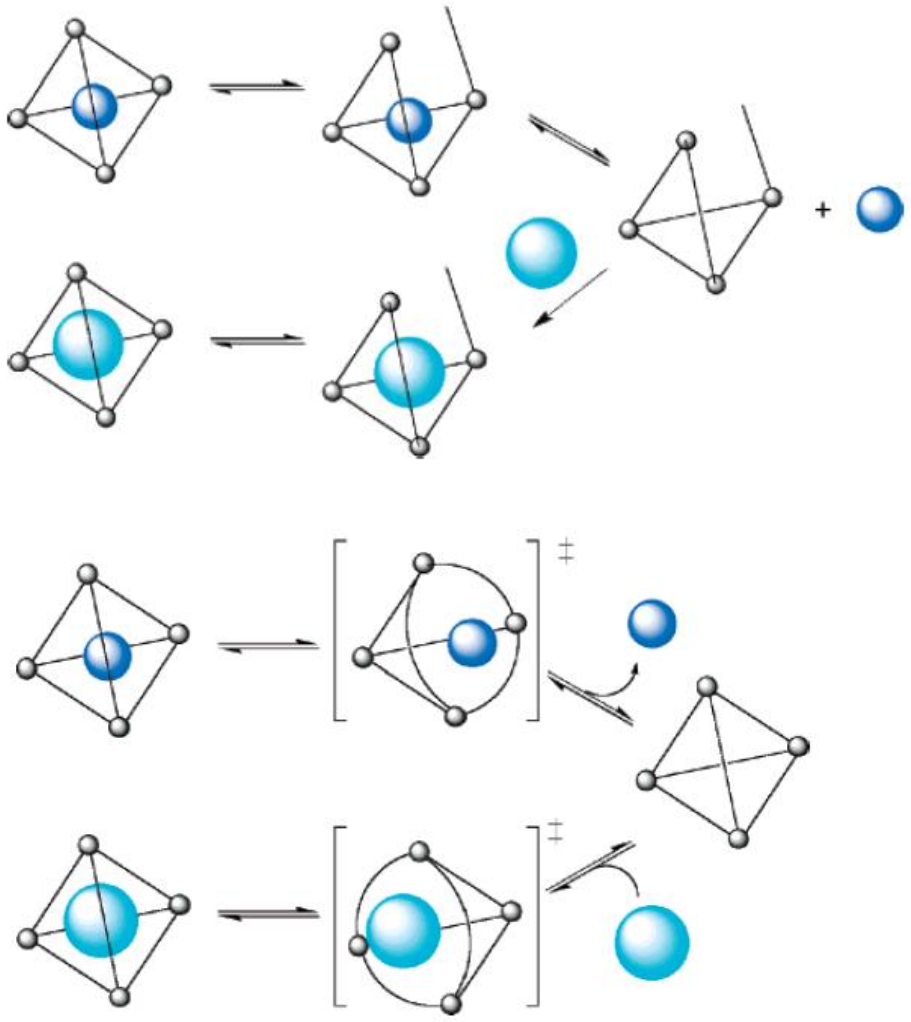

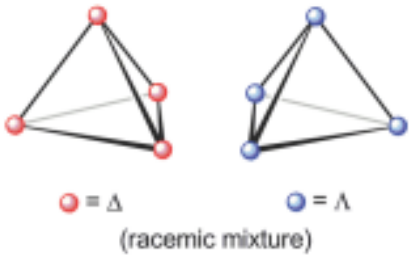

Resolution of the racemate using (−)-N′-methylnicotinium iodide: enantiopure ΛΛΛΛ-(S-nic ⊂ cage) and ΔΔΔΔ-(S-nic ⊂ cage) stereoisomers, after sequential ion exchange chromatography.

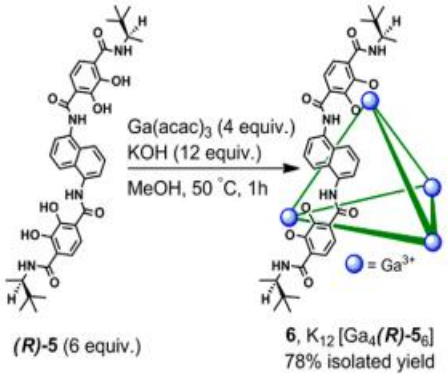

Achieving enantiopure M_4L_6 assembly without resolution using an amide-containing chiral directing group at the vertex of ligand - (*R*)-5 OR (*S*)-5.

6-$K_{12}Ga_4$(*R*)-5_6 and **6**-$K_{12}Ga_4$(R)-5_6 by CD spectroscopy: similar to those of ΔΔΔΔ-cage and ΛΛΛΛ-cage from racemate resolution.

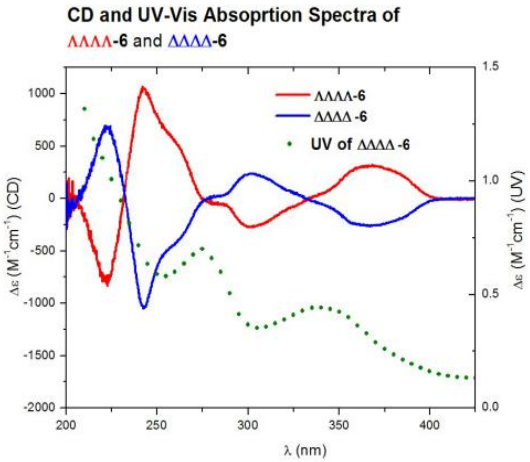

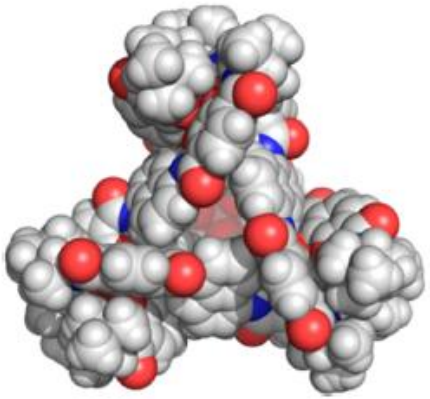

Figure 2. X-ray structure of ΔΔΔΔ-6.

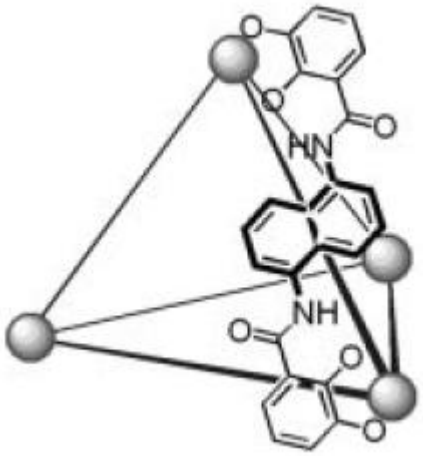

4

Addition of one equivalent of **4** to the $[Ga_4L_6]^{12-}$ assembly in D_2O results in the shift of the tropylium singlet from $\delta = 6.45$ to 2.95 ppm (Figure 4, a). Integration of this upfield-shifted tropylium signal indicates that this cation is encapsulated as a guest inside the tetrahedral assembly with a 1:1 ratio. Addition of a second equivalent of tropylium ion results in a second broad resonance at $\delta = 5.18$ ppm (Figure 4, b). The upfield shift of this resonance, compared to the resonance of free tropylium in D_2O, indicates that the second equivalent of aromatic tropylium cation interacts with the $[Ga_4L_6]^{12-}$ assembly by ion-pair association with the highly-charged assembly, as seen

After 20 h in solution (Figure 4, c), the encapsulated tropylium signal is still sharp, while the signal for the tropylium associated with the assembly was noticeably broadened, and the signal for free tropylium at $\delta = 6.45$ ppm is unobservable. Free tropylium completely decomposes in D_2O after approximately 24 h, so it seems that encapsulation of this cation in the hydrophobic environment of the $[Ga_4L_6]^{12-}$ cavity has significantly increased its stability.[26]

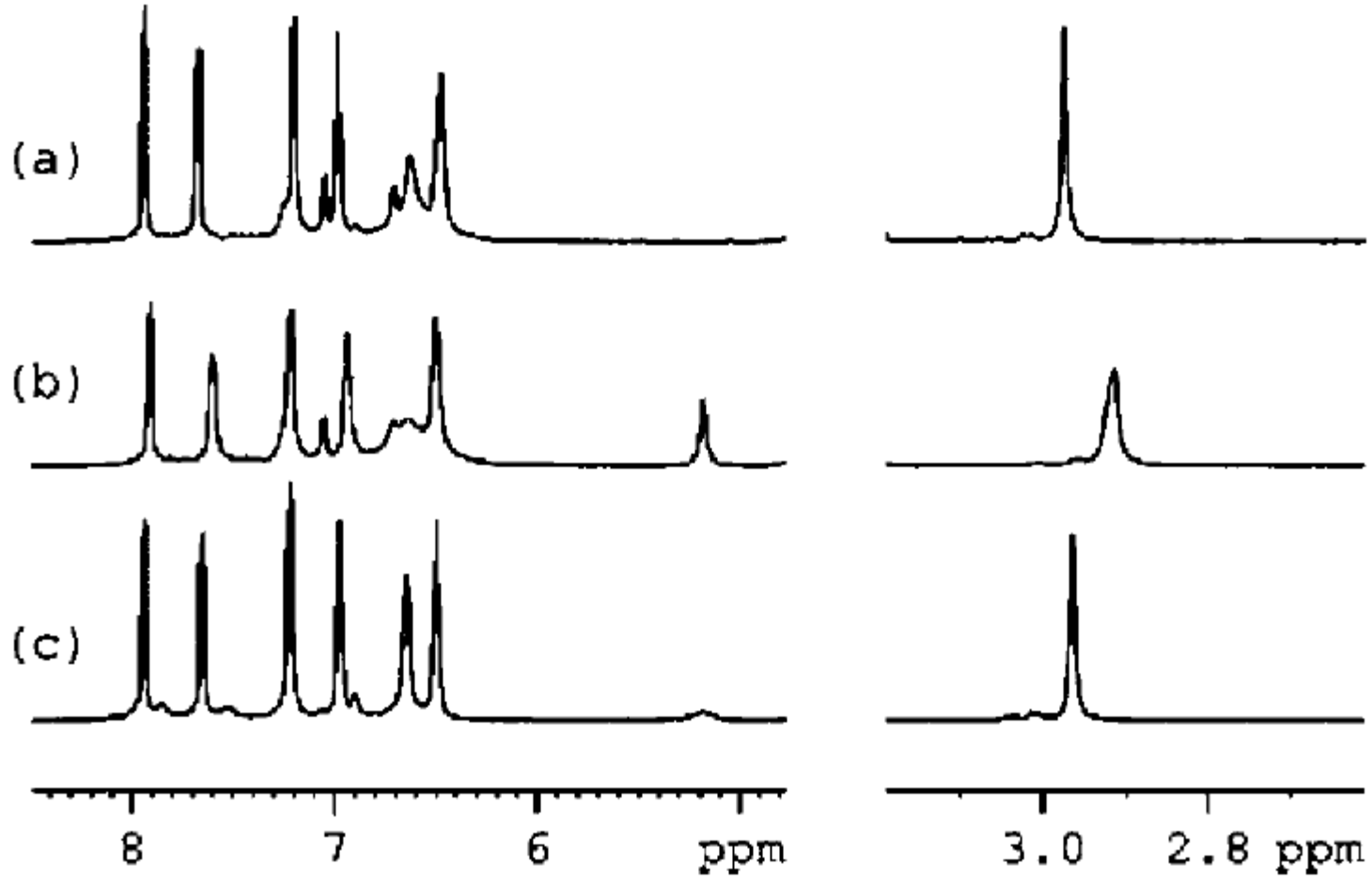

Figure 4. ^{1}H NMR spectra in D_2O of (a) the $[Ga_4L_6]^{12-}$ assembly + 1 equiv. **4**; (b) + 2 equiv. **4**; (c) sample in spectrum b after 20 h

Acid Catalysis in Basic Solution: A Supramolecular Host Promotes Orthoformate Hydrolysis

Michael D. Pluth, Robert G. Bergman,* Kenneth N. Raymond*

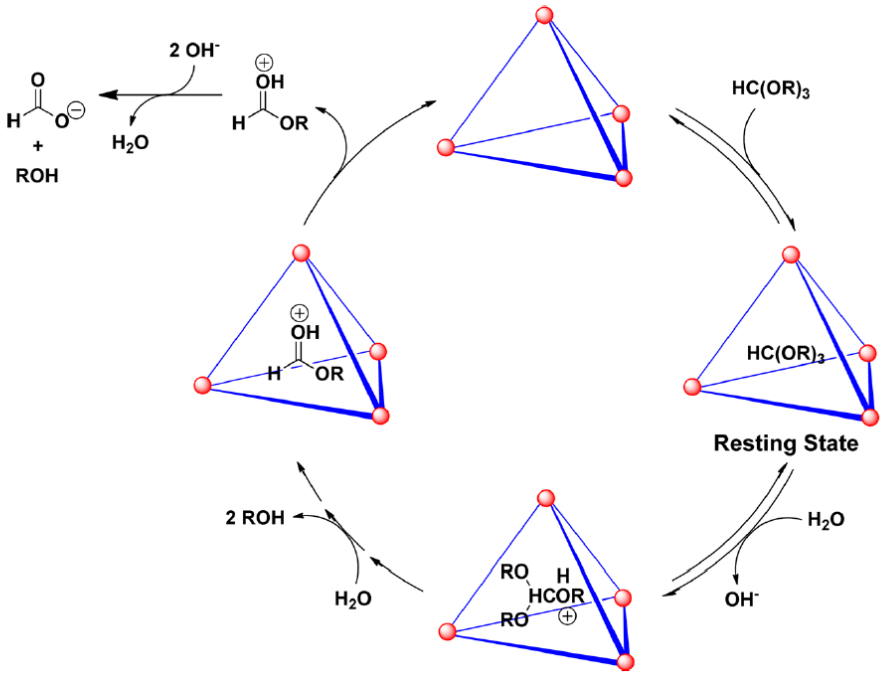

reached. Although the pK_a of **3**-H$^+$ is 10.8 in free solution, stabilization of the protonated form by **1**, which can be calculated as the product of the pK_a and the binding constant of the protonated amine, shifts the effective basicity to 14.3 (*32*). This dramatic shift highlights the substantial stabilization of the protonated species over the neutral species upon encapsulation in the highly charged cavity (*33*).

Inclusion of neutral substrate – protonation by water – two hydrolitic steps within the cavity (2 equiv of alchol released) – protonated formiate released and deprotonated in solution by the base – concomitant release of free cage.

ChemComm

Chemical Communications

www.rsc.org/chemcomm

Volume 49 | Number 25 | 28 March 2013 | Pages 2465–2580

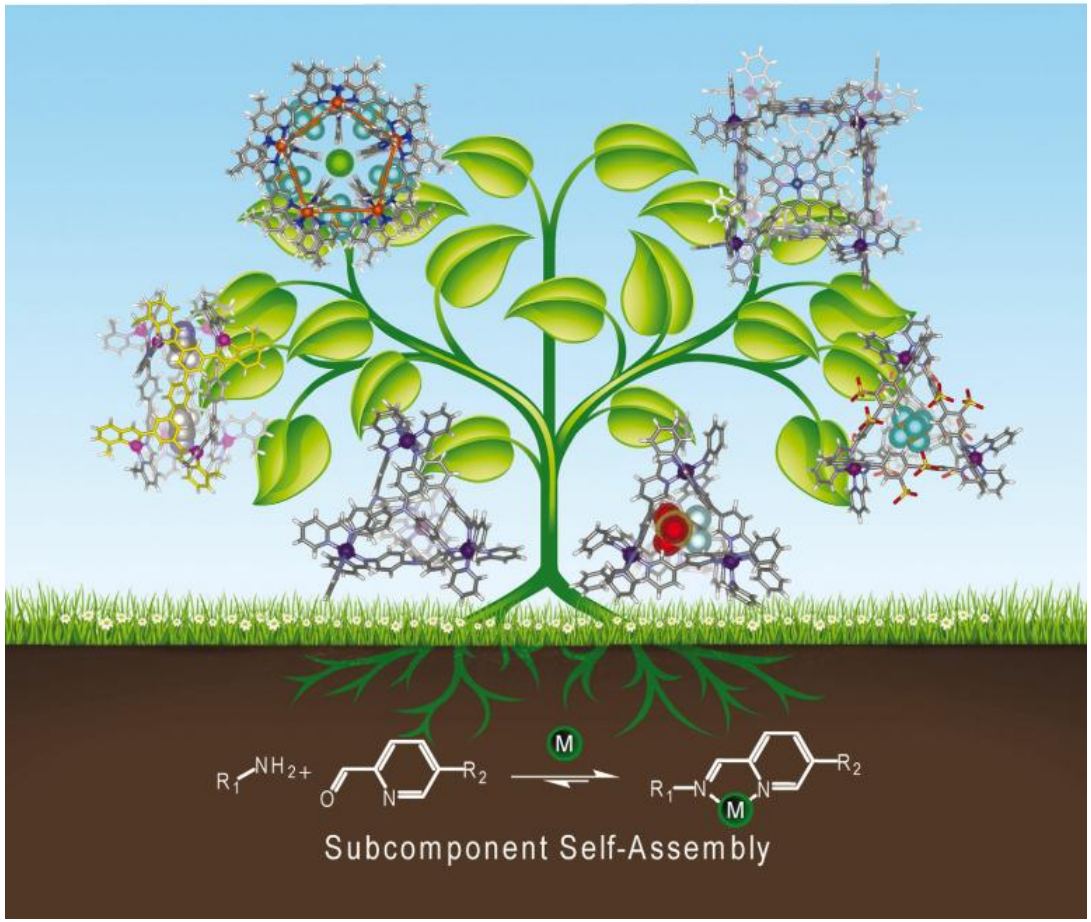

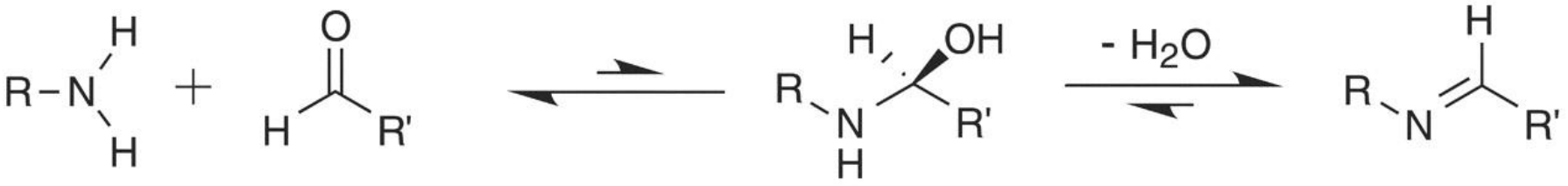
- H_2O
Hemiaminal
Imine

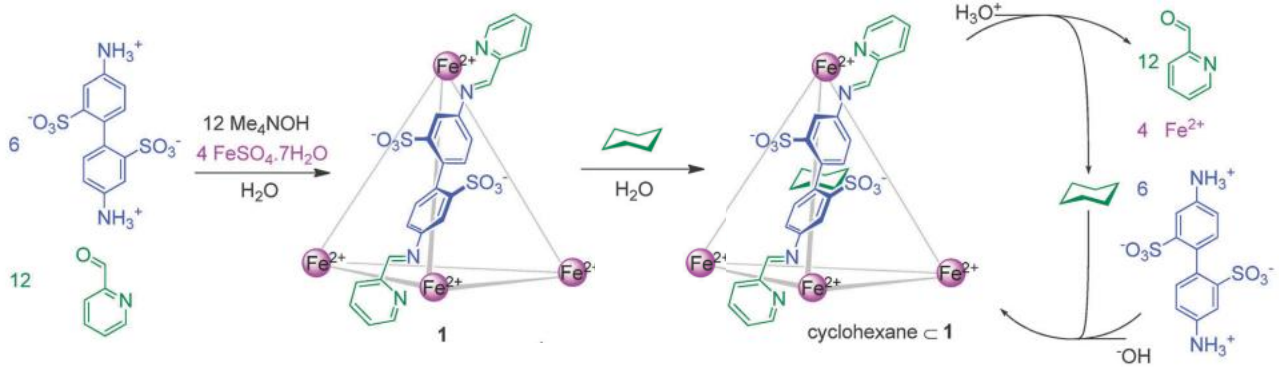
12 Me_4NOH
4 $FeSO_4.7H_2O$
H_2O
1
H_2O
cyclohexane ⊂ 1
H_3O^+
^-OH

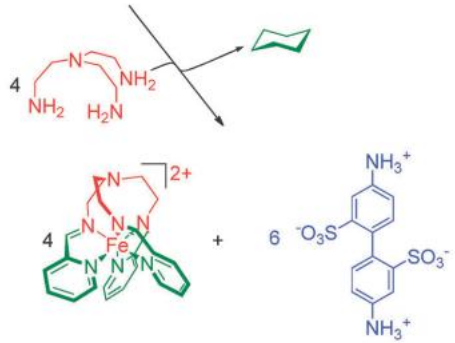

4,4’-diaminobiphenyl/2’-carboxyaldheyde

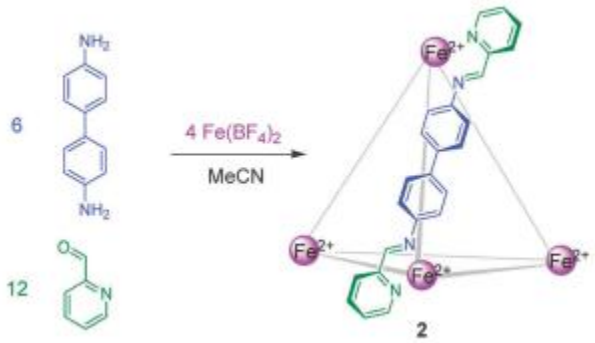

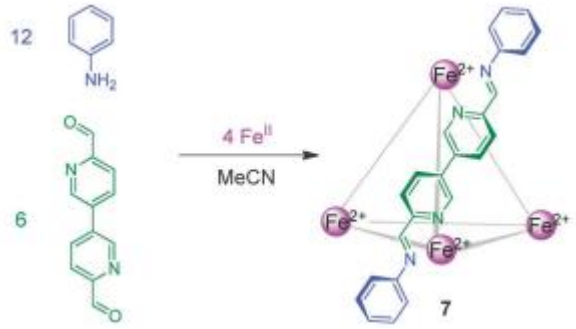

6,6’-diformyl-3,3’-bipyridinel/aniline

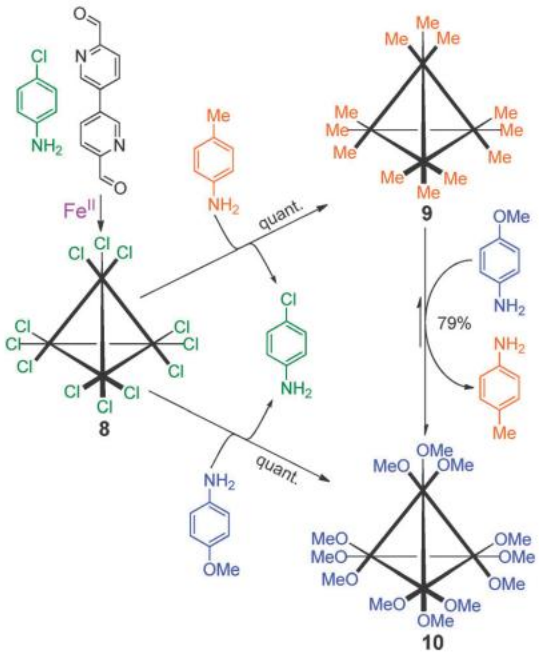
Fe^{II}
quant.
quant.
79%
8
9
10

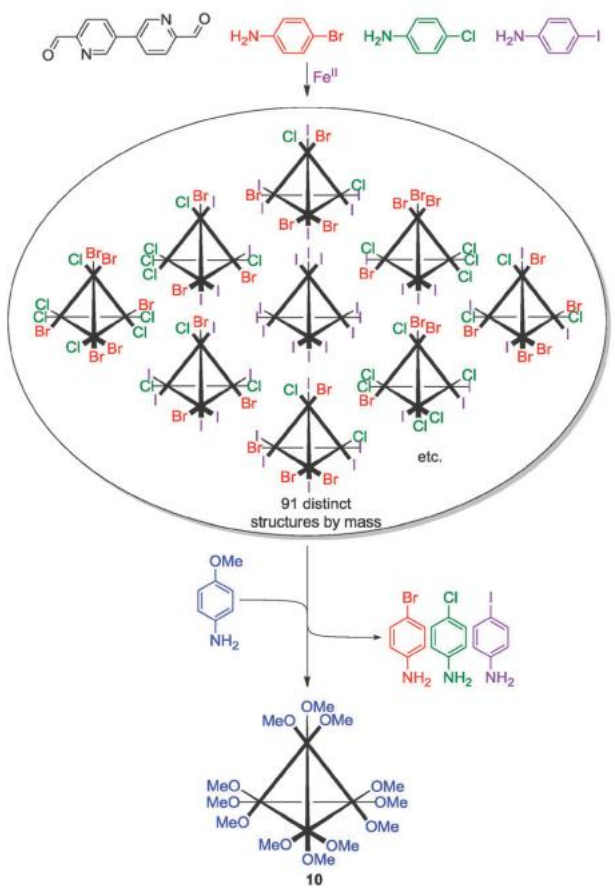
Fe^{II}
91 distinct
structures by mass
etc.
10

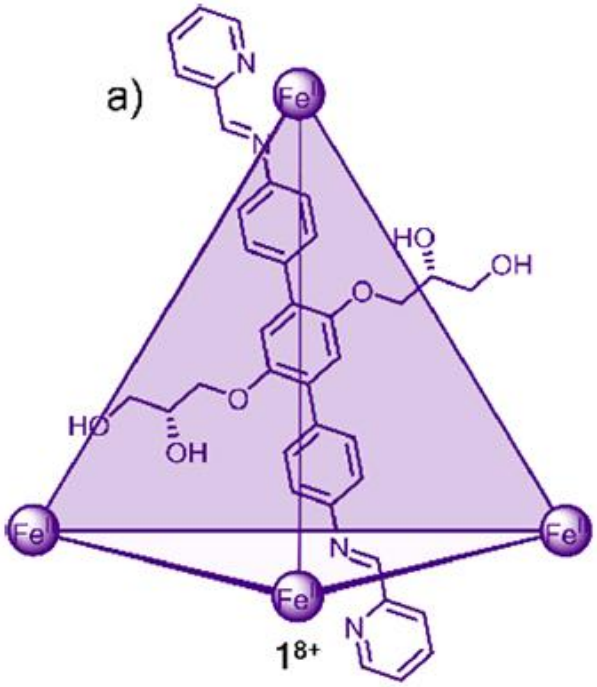

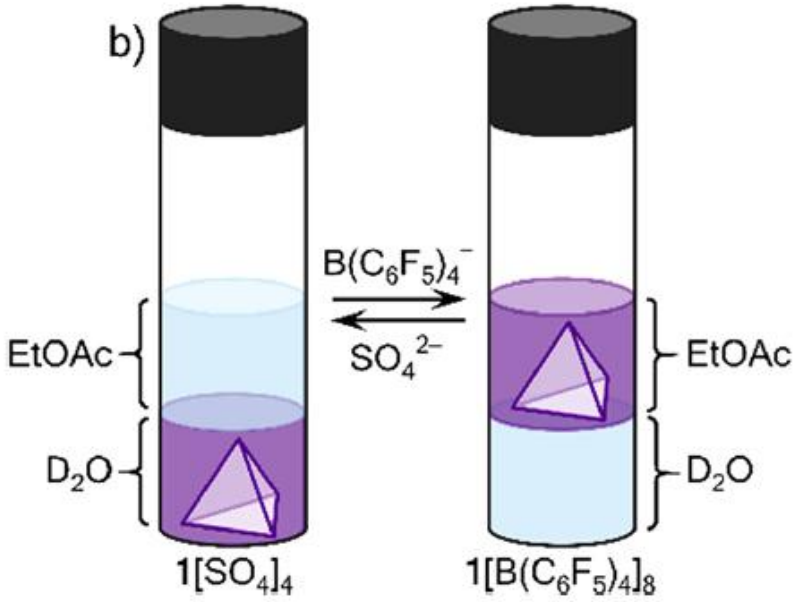

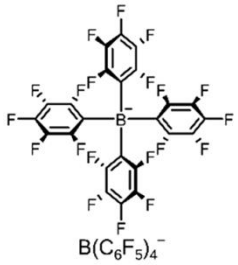

$LiB(C_6F_5)_4$ to promote anion metathesis from SO_4^{2-} to $B(C_6F_5)^{4-}$

$(n\text{Bu}_4\text{N})_2SO_4$ to regenerate the solfate cage

Tris-pentafluoroborane

White Phosphorus Is Air-Stable Within a Self-Assembled Tetrahedral Capsule

Prasenjit Mal,[1] Boris Breiner,[1] Kari Rissanen,[2] Jonathan R. Nitschke[1]*

SCIENCE VOL 324 26 JUNE 2009

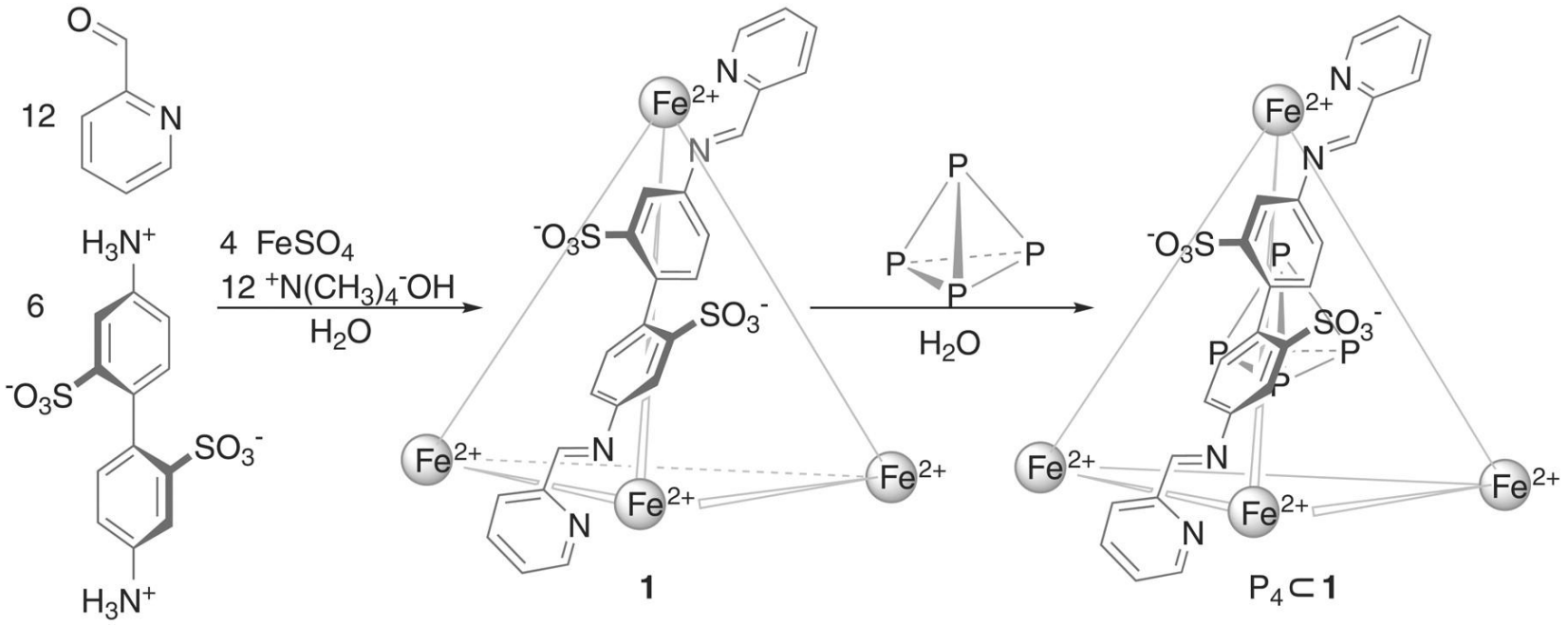

Fig. 1 Synthesis of tetrahedral cage 1 and subsequent incorporation of P4.

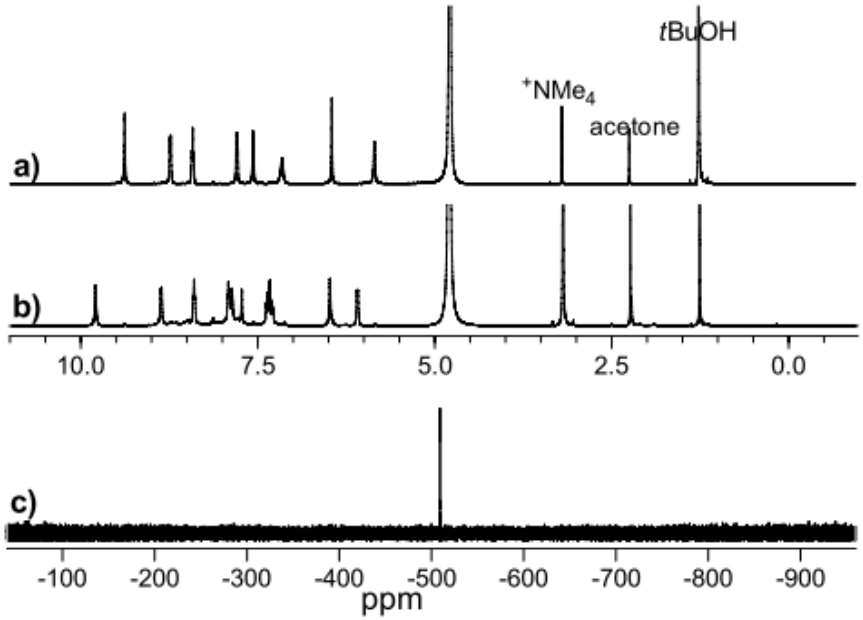

Figure S1. ^{1}H NMR spectra in D_2O of cage **1** (top), of $P_4\subset$**1** (middle), and ^{31}P NMR spectrum of $P_4\subset$**1** (bottom).

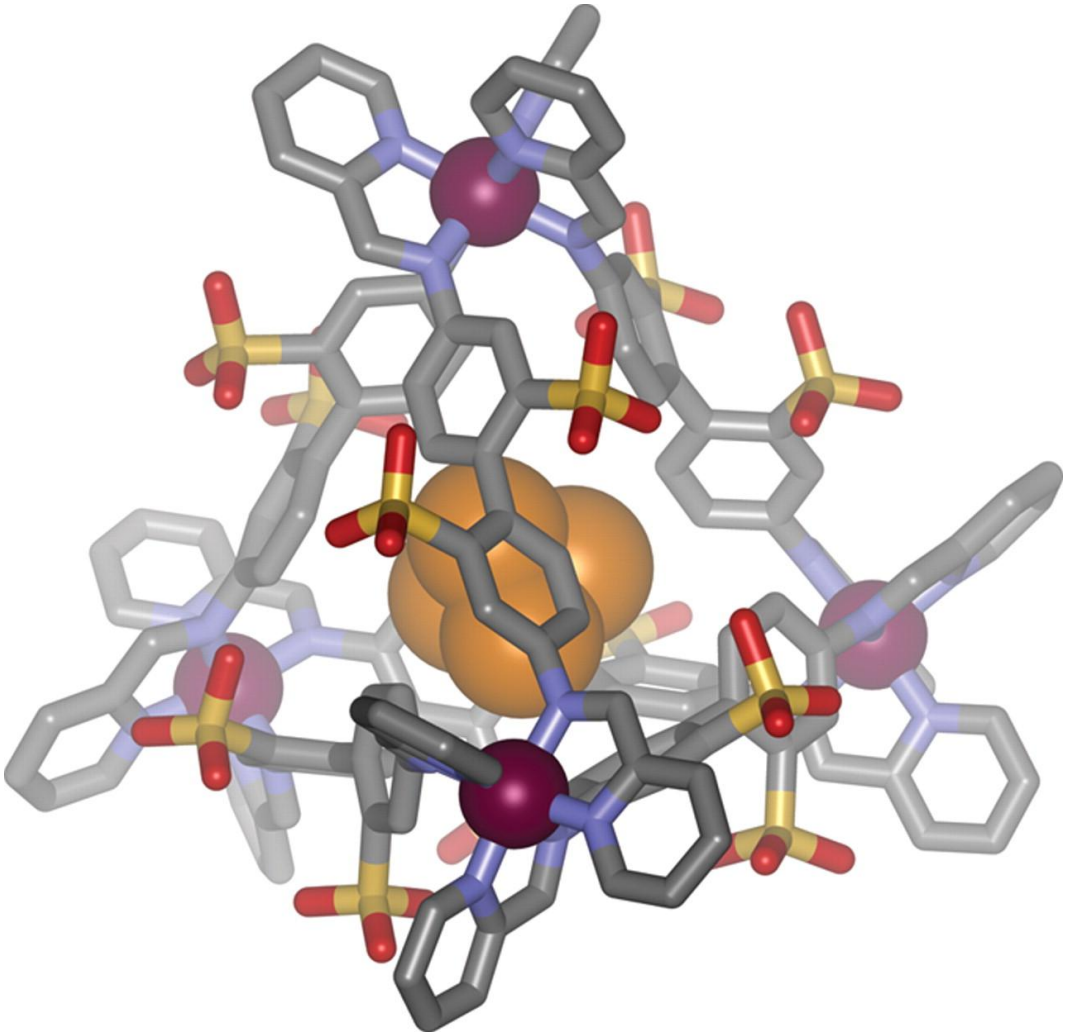

Fig. 2 Crystal structure of P4⊂1.

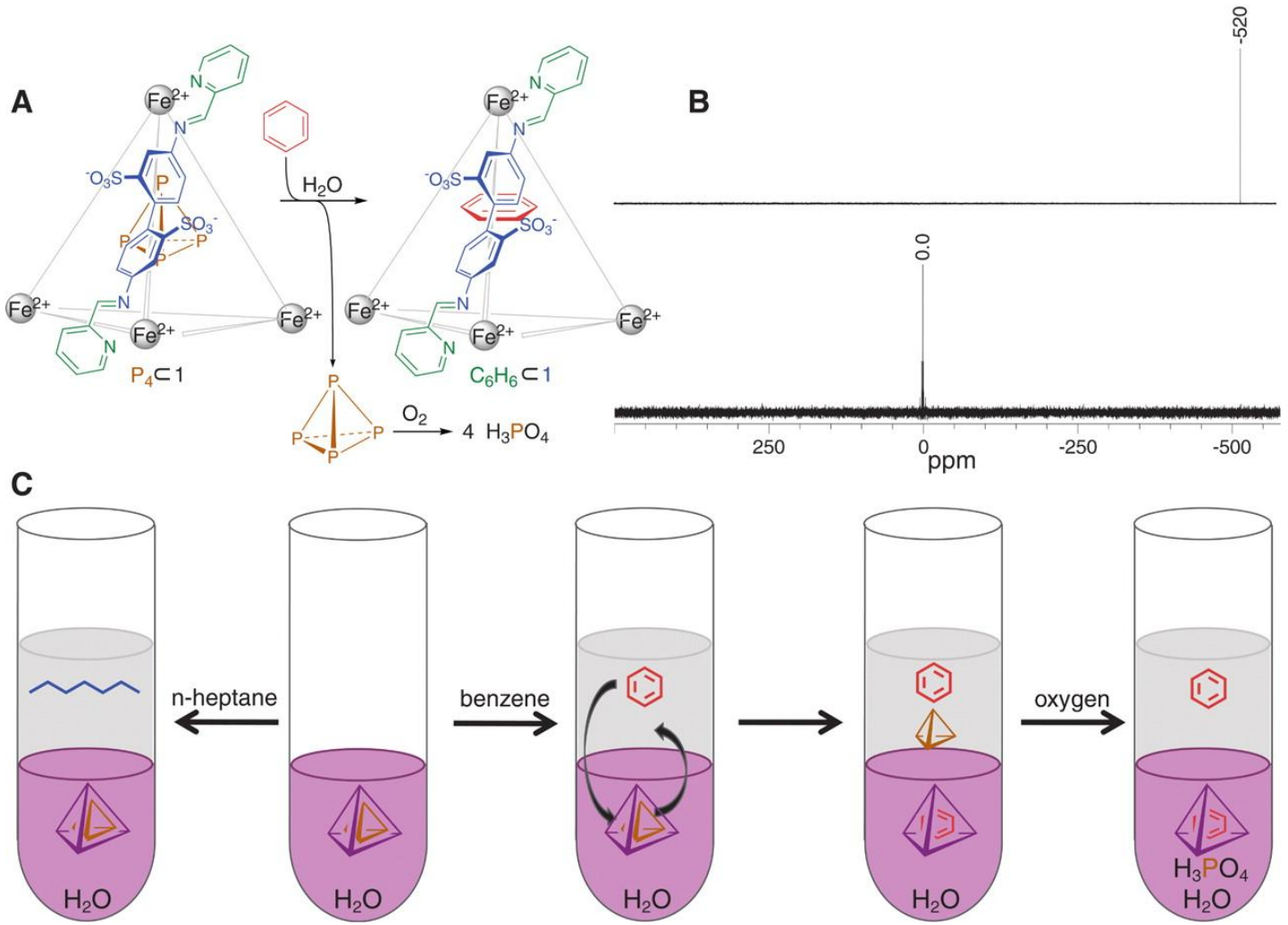

Fig. 3 Extraction of P4 from 1 by n-heptane is not possible, whereas replacing P4 with another suitable guest (benzene or cyclohexane) results in the facile removal of P4 into the organic solvent.

https://www.nitschkegroup-cambridge.com/research-areas

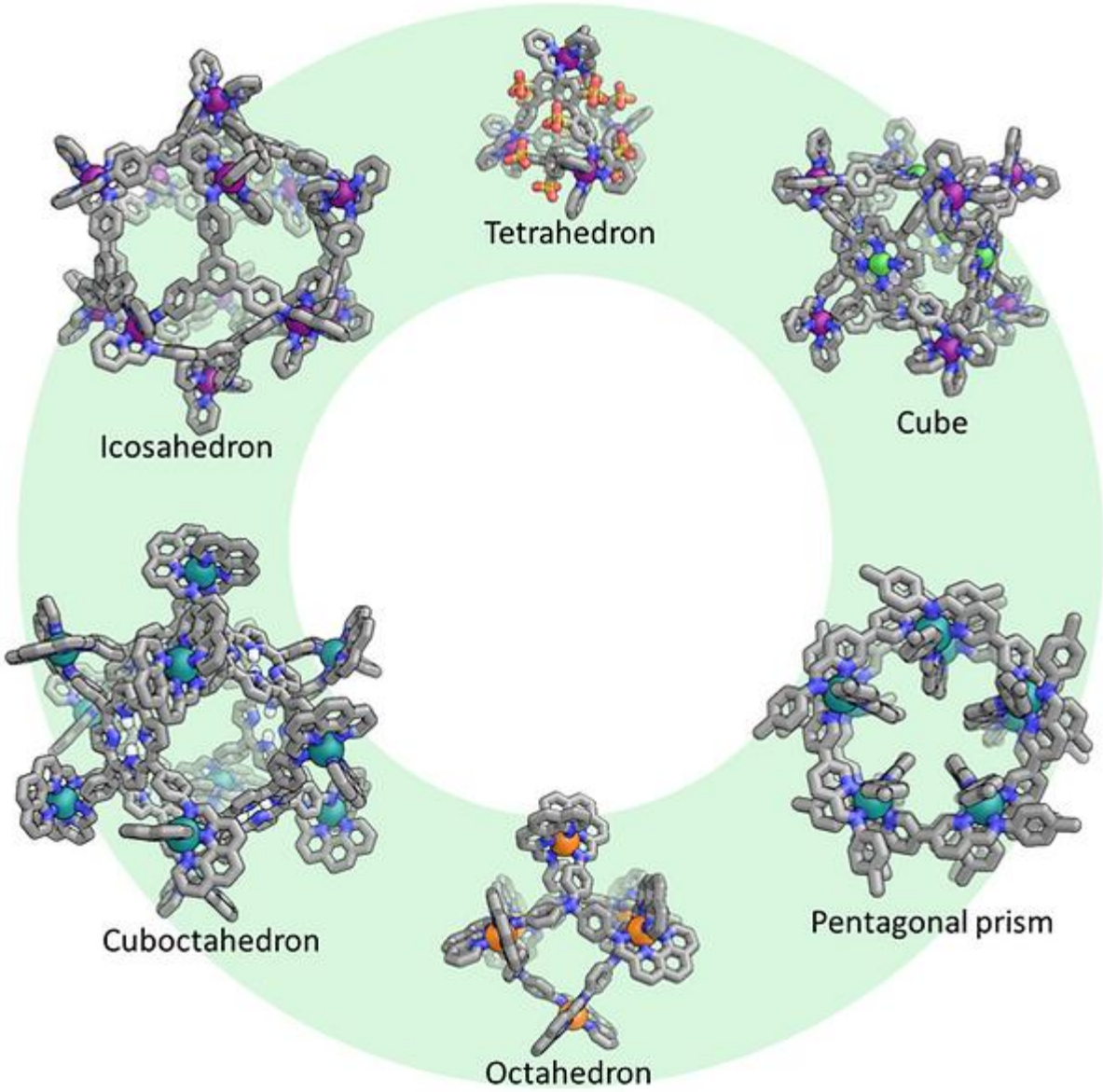

Design and Applications of Water-Soluble Coordination Cages

Edmundo G. Percástegui, Tanya K. Ronson, and Jonathan R. Nitschke*

Cite This: *Chem. Rev.* 2020, 120, 13480–13544

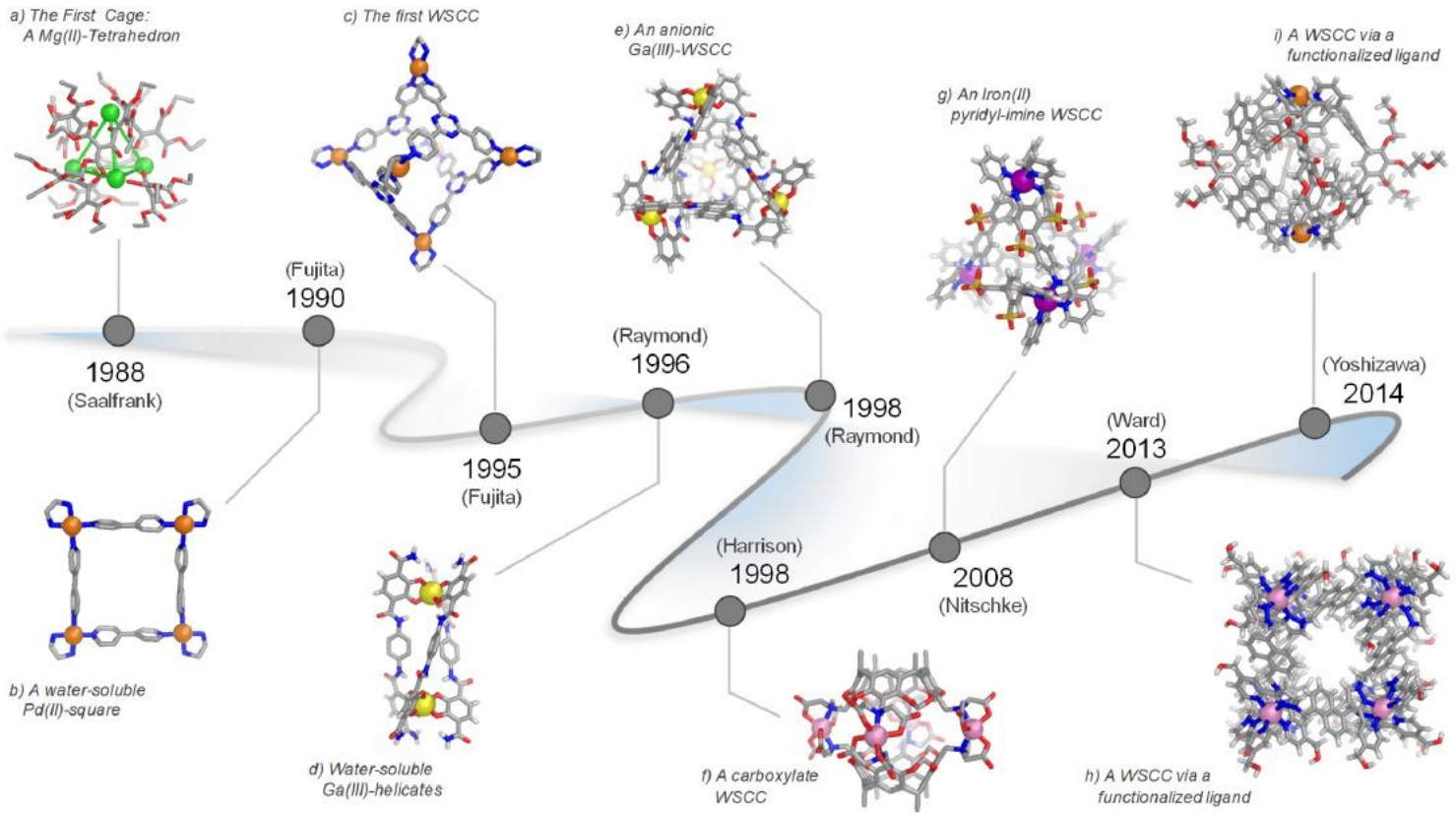

Figure 1. Timeline showing major advances in supramolecular coordination chemistry that have led from (a) the first cage complex to (b–f) early water-soluble complexes in the 1990s, and to (g–i) recent examples of WSCCs synthesized from ligands functionalized with solubilizing functional groups. The name of the group for each work is shown for reference.

Choice of metal ion - coordination geometry + kinetic lability:

Octahedral - Ga^{III}, Al^{III}, Ti^{IV}, Fe^{II}, Co^{II}, Zn^{II}, Cd^{II}, $Ni^{II;}$
Square planar - Pd^{II} and Pt^{II}
Lanthanide ions kinetically labile BUT variable coordination number and geometry
Kinetically inert metal ions (e.g. Ru^{II} and Ir^{III}): kinetic control unless *trans* effect.

The self-assembly process - interplay between enthalpy and entropy:

multiple equilibria/variety of factors - metal coordination geometry/kinetic lability/ligand geometry/metal-to-ligand stoichiometry/concentration/solvent/presence of guests.
Therefore, it can be difficult to predict the outcome since there is a delicate balance.

The principle of maximum site occupancy:

species where all the metal coordination sites are occupied with ligands are more stable than those with vacant coordination sites since this maximises the number of metal–ligand bonds and therefore, the enthalpy.

On the other hand, a system containing a larger number of smaller cages with fewer building blocks is favored on entropic grounds over one containing a smaller number of larger cages.

Multiple architectures can be self-assembled from the same building blocks:
(a) a single cage when it is the thermodynamically most stable structure;
(b) a mixture of cages as the thermodynamic products with the distribution reflecting the relative energies of the cages;
(c) a dynamic combinatorial library with a large number of interconverting species in equilibrium.

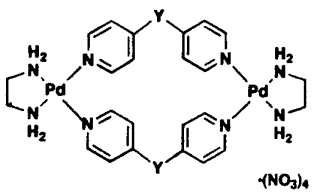

$\cdot(NO_3)_4$

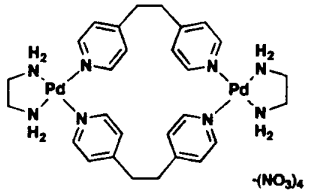

$\cdot(NO_3)_4$

Y = CH_2

Y = $C(OH)_2$

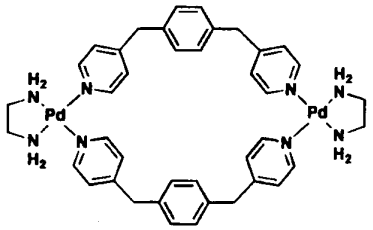

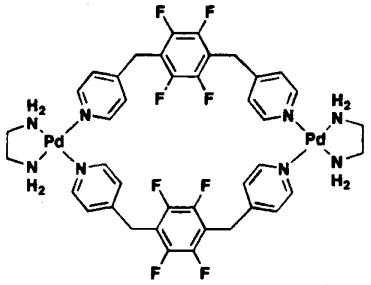

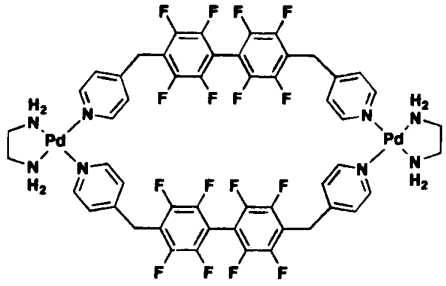

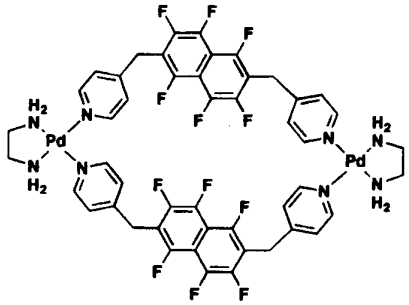

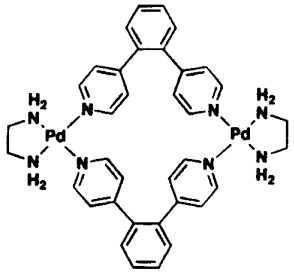

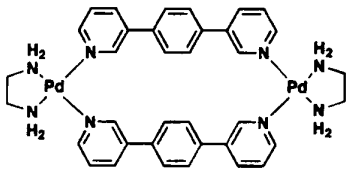

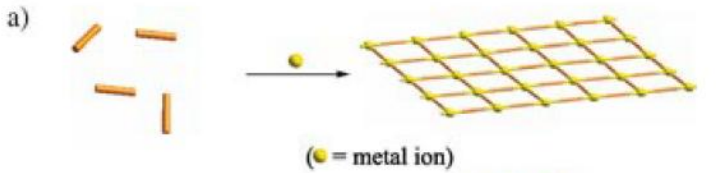
a)
(● = metal ion)

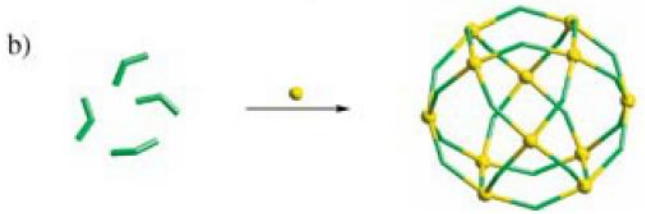
b)

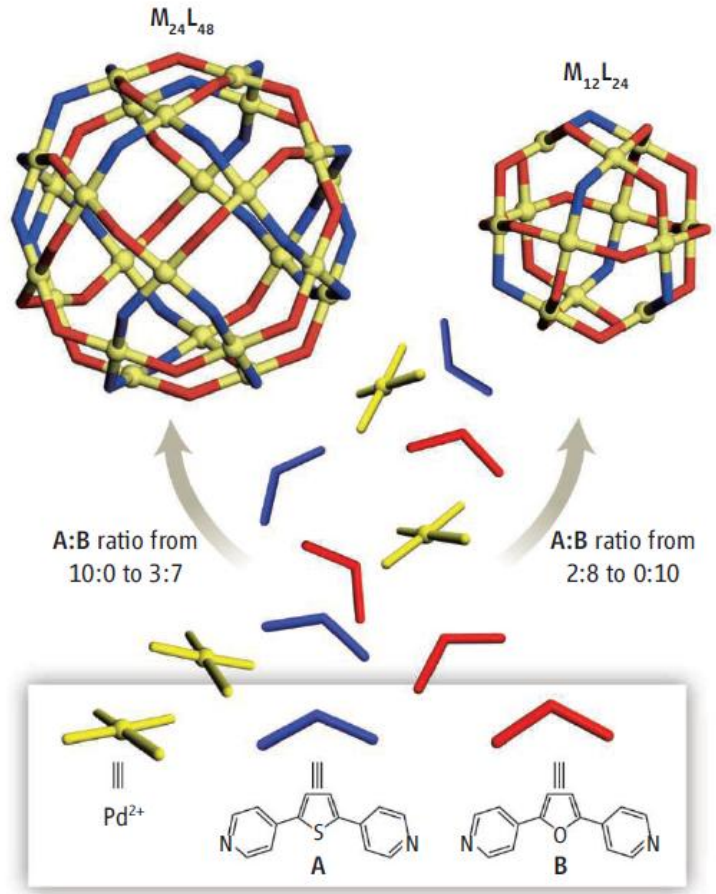
M24L48
M12L24
A:B ratio from
10:0 to 3:7
A:B ratio from
2:8 to 0:10
Pd2+
N
S
N
A
N
O
N
B

Design of lower symmetry cages

- symmetry breaking of the ligand upon metal coordination
- self-assembly of heteroleptic cages containing multiple ligands
- use of non-symmetric ligands to form homoleptic but lower symmetry cages
- use of multiple metals to form heterometallic cages.

Self-Sorting

narcissistic self-sorting - homoleptic cages with one ligand type in each cage
statistical mixture - both ligands are incorporated into the cages according to their statistical distribution;
integrative self-sorting - a nonstatistical distribution of heteroleptic cages results.

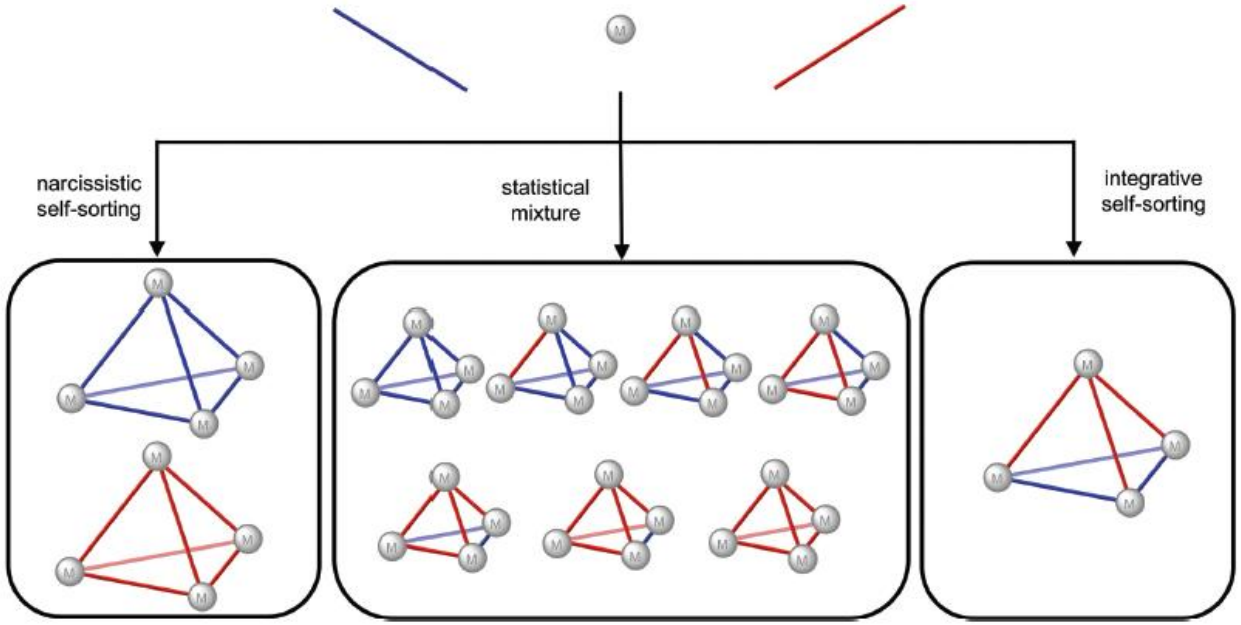

The key challenges to the design of heteroleptic cages via integrative self-assembly are, therefore, stabilisation of the heteroleptic cage/s relative to the homoleptic cages and biasing the system away from the statistical mixture.